

T-70-17853
CR-66909

DESIGN OF DISK-GAP-BAND AND MODIFIED RINGSAIL
PARACHUTES AND DEVELOPMENT OF BALLUTE
APEX INLET FOR SUPERSONIC APPLICATION

By G. L. Faurote

Distribution of this report is provided in the interest of information exchange. Responsibility for the contents resides in the author or organization that prepared it.



Prepared under Contract No. NAS1-8564 by
GOODYEAR AEROSPACE CORPORATION
Akron, Ohio

for

Langley Research Center
NATIONAL AERONAUTICS AND SPACE ADMINISTRATION

FOREWORD

Work described in this document was performed by Good-year Aerospace Corporation, Akron, Ohio, under NASA Contract NAS1-8564, Ground-Test Decelerator Program. The contractor's number for this report is GER-14657.

CONTENTS

		<u>Page</u>
FOREWORD		iii
ILLUSTRATIONS		vii
TABLES		xi
SUMMARY		1
<u>Section</u>	<u>Title</u>	
I	INTRODUCTION	1
II	DESIGN CONDITIONS	2
III	DESIGN CONSIDERATIONS	3
	General	3
	DGB Pattern and Design Data	3
	DGB Stress Analysis	5
	Ringsail Gore Pattern and Design Data	16
	Ringsail Stress Analysis	27
	BALLUTE Inlet Design	32
	General	32
	Inlet Sizing.	32
	Static Inflation Tests	37
	Connector Link, Riser, Swivel, and Bridle	40
	Decelerator Packing Scheme	42
	Parachute	42
	BALLUTE	42
	Material Selection for Fabric Decelerators	46
	Pressure Model Design	46
	General	46
	BALLUTE Design	46
	BALLUTE Stress Analysis.	46
	Parachute Design.	53
	Parachute Stress Analysis.	53
IV	DESIGN DOCUMENTATION	60
V	MANUFACTURING CONSIDERATIONS	95
VI	CONCLUDING REMARKS	95

<u>Appendix</u>	<u>Title</u>	<u>Page</u>
A	BALLUTE INFLATION ANALYSIS	96
	Inflation Model	96
	Calculating Procedure.	97
	SYMBOLS	98
	REFERENCES	100

ILLUSTRATIONS

<u>Figure</u>	<u>Title</u>	<u>Page</u>
1	Comparison of Parachute Gore Patterns	4
2	DGB Inflated Geometry	9
3	Cross-Section of Band Gore Lobe	9
4	Free-Body Diagram of Band and Disk Reinforce- ment Band	11
5	Vent Geometry	11
6	Cross Section of Vent Gore Lobe	12
7	Disk Gore Cross Seam	15
8	Basic Ringsail Geometry	17
9	Basic Gore Dimensions for the 5.5-Ft Ringsail . .	19
10	Fullness Added to 5.5-Ft Ringsail	20
11	Ring and Sail Patterns for the 5.5-Ft Ringsail . . .	20
12	Parachute Stability Regions	21
13	Basic Gore of the 5.5-Ft Ringsail	23
14	Scoop Shape	24
15	Geometry of Gap	26
16	Geometry of Sail Scoop	26
17	Ringsail Inflated Geometry	30
18	Free-Body Diagram of Skirt Reinforcement Band .	30
19	Free-Body Diagram of Vent Reinforcement Band .	31
20	Predicted Wake Properties Aft of 120-Deg Cone .	33
21	Apex Inlet and Valve Design	34
22	Blockage of Inlet by Meridional Extensions	35
23	Flow Entering Apex Inlet	36

<u>Figure</u>	<u>Title</u>	<u>Page</u>
24	Predicted Ratio of Wake Total Pressure to Free-Stream Static Pressure for 120-Deg Cone	37
25	BALLUTE Internal Pressure Coefficient versus Free Stream	39
26	BALLUTE Leak Rate versus Internal Pressure	40
27	Parachute Folded Longitudinally	43
28	Parachute in Deployment Bag	43
29	Retaining Loop Arrangement	44
30	BALLUTE Folded Longitudinally	45
31	BALLUTE in Deployment Bag	45
32	BALLUTE Pressure Model	48
33	Normal Force Acting on BALLUTE	50
34	Free-Body Diagram of Yoke Member	51
35	Free-Body of Model Attachment Screw	52
36	DGB Pressure Model	54
37	Front Section of Canopy in Flat Condition	54
38	Cross Section of Pressure Model	55
39	Assumed Distribution of Normal Force	57
40	Cross Section of Elements Connecting Disk and Band	57
41	Geometry of Connecting Element	58
42	Element 9	59
43	Disk-Gap-Band Parachute Assembly, 5.5-Ft D ₀ (Drawing 655A-001, Sheets 1 through 4).	61
44	Ringsail Parachute Assembly, 5.5-Ft D ₀ (Drawing 655A-002, Sheets 1 and 2)	69

<u>Figure</u>	<u>Title</u>	<u>Page</u>
45	BALLUTE, 48-In. -Diameter Burble Fence (Drawing 655A-003, Sheets 1 through 5)	73
46	Parachute Deployment Bag (Drawing 655A-005) . . .	83
47	BALLUTE Deployment Bag (Drawing 655A-006) . . .	85
48	Disk-Gap-Band Parachute and BALLUTE Pressure Models (Drawing 655A-007, Sheets 1 through 4) . . .	87
49	BALLUTE Inflation Model	96

TABLES

<u>Table</u>	<u>Title</u>	<u>Page</u>
I	Decelerator Loading Conditions	2
II	Summary of DGB Constructed and Actual Geometric Properties	6
III	Strength-Loss and Safety Factors (DGB Parachute) .	7
IV	Sail Dimensions for the 5.5-Ft Ringsail.	18
V	Strength-Loss and Safety Factors (Ringsail Parachute)	28
VI	Strength-Loss and Safety Factors (Ancillary Equipment)	41
VII	Decelerator Materials Summary	47
VIII	Moments of Inertia	59
IX	Major Decelerator Components.	60

DESIGN OF DISK-GAP-BAND AND MODIFIED RINGSAIL
PARACHUTES AND DEVELOPMENT OF BALLUTE
APEX INLET FOR SUPERSONIC APPLICATION

By G. L. Faurote
Goodyear Aerospace Corporation

SUMMARY

Goodyear Aerospace Corporation (GAC) has designed and fabricated flexible wind-tunnel decelerator configurations for use by NASA Langley Research Center (NASA/LRC) in its Ground Test Decelerator Program. The models furnished by GAC included fabric disk-gap-band and ring-sail parachutes and ram-air-inflated towed BALLUTES.^a In addition, Goodyear Aerospace has designed disk-gap-band and BALLUTE solid pressure models. All configurations were designed for test in a supersonic-flow regime.

I - INTRODUCTION

Prior investigations have shown the feasibility of using inflatable decelerators to facilitate planetary entry and landing when a basic atmosphere exists (References 1 through 3). Such investigations also have shown that this type of auxiliary decelerator provides an efficient and economical means for accomplishing the required retardation. As a result, various candidate decelerator configurations are currently undergoing test and evaluation by NASA/LRC to determine their overall suitability. In support of this effort, a Ground Test Decelerator Program is being implemented by NASA/LRC. The purpose of this program is (1) to increase the basic understanding of the effects of such variables as Mach number, geometric porosity, and forebody-to-decelerator-diameter ratio on the reefed and full-open supersonic performance of parachutes; (2) to determine the feasibility of decreasing BALLUTE inflation times with an apex inlet; and (3) to compare wind-tunnel and flight-test data. In addition to the current evaluation of the trailing BALLUTE and parachute configurations, a separate effort investigating the suitability of the attached inflatable decelerator (AID) for augmenting basic entry vehicle drag and stability characteristics is being conducted by NASA/LRC (References 3 and 4).

Goodyear Aerospace has designed and fabricated the following wind tunnel test models for use in this program:

1. Twelve disk-gap-band (DGB) parachutes (canopies with three geometric porosities were fabricated to enable the study of porosity effects)

^aTM, Goodyear Aerospace Corporation, Akron, Ohio.

2. One ringsail parachute
3. Three BALLUTES with four ram-air side inlets
4. Two BALLUTES with four ram-air side inlets and a single apex inlet

As part of this program, Goodyear Aerospace also has designed rigid DGB and BALLUTE pressure models for wind-tunnel pressure distribution investigations.

Details of each configuration design with supporting analyses, in-plant testing, materials selection, and fabrication considerations, are discussed in the following sections of this report. A summary of the testing phase of the program, with detailed test conditions and performance parameters delineated, is presented in Reference 5.

II - DESIGN CONDITIONS

Each decelerator configuration was designed capable of withstanding the applicable loading conditions presented in Table I.

TABLE I - DECELERATOR LOADING CONDITIONS

Decelerator type	Size*	Loading conditions*	
		Drag coefficient	Dynamic pressure (psf)
DGB (fabric model)	$D_o = 5.5 \text{ ft}$	$C_{D_o} = 1.0$	70
Ringsail (fabric model)	$D_o = 5.5 \text{ ft}$	$C_{D_o} = 1.0$	70
BALLUTE envelope (fabric model)	$D_E = 40 \text{ in.}^+$	$C_{D_E} = 1.1$	120
Riser - Bridle	$D_E = 40 \text{ in.}^+$	$C_{D_E} = 1.4$	120
DGB solid model	$D_{\text{max}} = 6 \text{ in.}$...	500
BALLUTE (solid model)	$D_{\text{max}} = 6 \text{ in.}$...	500

* Contract requirement.

+ BALLUTE equator diameter.

As reflected in Section I, the purpose of the current program is related to obtain aerodynamic characteristics of these decelerator configurations. It is noted that several minutes of decelerator operation, at the deployment dynamic

pressure will be required to permit the effect of Mach number variations on decelerator performance to be made. In view of the program's purpose and the required length of decelerator operation, a conservative approach, compared to that which is typically used in the design of flight systems, was adopted in the decelerator designs discussed in the following section.

III - DESIGN CONSIDERATIONS

General

The design of each decelerator type reflects, to the extent possible, consideration of the details of decelerator systems tested during NASA/LRC's flight test programs (References 1 and 6). Similarity to the flight-tested hardware was a primary design goal and is believed to be essential if reasonable comparison of performance data is expected. The similarity between models of any one configuration was considered equally important in ensuring that the test results will be meaningful as applied to increasing the basic understanding of decelerator-forebody aerodynamics and dynamics.

DGB Pattern and Design Data

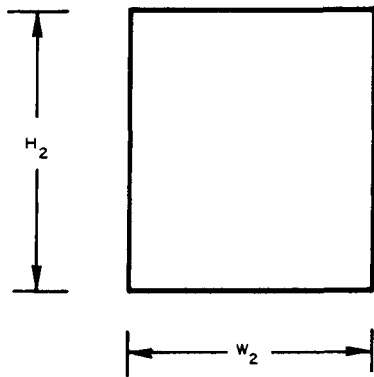
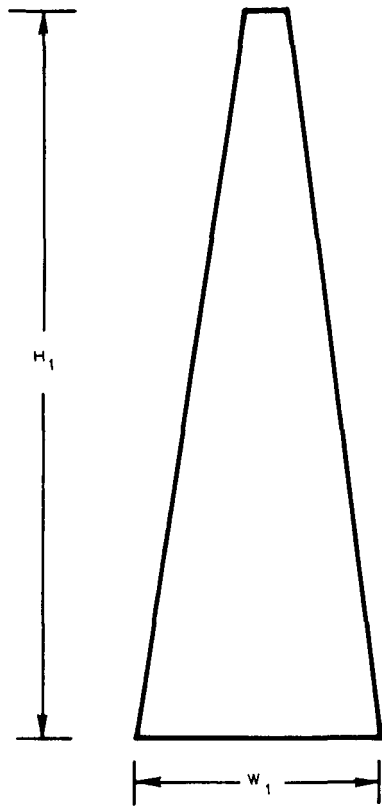
The method of Reference 7 was used to establish the basic parachute gore pattern (for $\lambda_g = 12.5$ percent) except where consideration of scale dictated variations to ensure proper decelerator performance.

Selection of the number of gores to be used in the parachute was based on retaining the existing full-scale proportionality between the band gore width (W_2) and the band gore height (H_2) and the proportionality between the disk gore width at the gap (W_1) and the disk gore height (H_1). Retaining these proportionalities will ensure that the inflated profile of the 5.5- and 40-ft parachutes will be as similar as possible.

It may be shown that the desired proportional relationships are essentially obtained through the use of 32 gores for the geometric porosity case of 12.5 percent.

Only small variations occur in the case of the 10.0- and 15.0-percent geometric porosities. The gore patterns and above-discussed proportionalities for both the 40- and 5.5-ft configurations ($\lambda_g = 12.5$ percent) are presented in Figure 1 for purposes of comparing the geometric properties.

The 10- and 15-percent geometric porosity designs retained the disk geometry of the 12.5-percent geometric porosity design. The gap was decreased and the band correspondingly increased to achieve the 10-percent geometric porosity; the reverse was done to achieve the 15-percent geometric porosity. Thus, each of the three geometric porosity designs used the same nominal diameter.



* PRIOR TO ADDING FULLNESS

GEOMETRIC PARAMETER	VALUE*	
	D _o = 40 FT	D _o = 5.5 FT
H ₁ (IN.)	174.530	24.030
w ₁ (IN.)	34.352	4.710
H ₂ (IN.)	57.620	7.903
w ₂ (IN.)	34.352	4.710
H ₁ /w ₁	5.100	5.100
H ₂ /w ₂	1.680	1.680

Figure 1 - Comparison of Parachute Gore Patterns

It should be noted that the referenced method used to determine the basic gore pattern does not account for the reduction in geometric porosity that results from the radial tapes passing over the gap or vent. In the case of the 40-ft nominal diameter model, this reduction in geometric porosity is approximately 0.30 percent of S_0 . However, in the case of the 5.5-ft design, the reduction is greater because the size of the radial tapes does not scale by the same ratio as the diameters.

This reduction in geometric porosity and other pertinent design data for each DGB parachute are summarized in Table II. The data, presented for each DGB fabricated, are referenced by serial number to permit variances in fabrication to be accounted for in evaluating relative parachute performance.

To ensure proper decelerator performance, blockage by the vent radials was considered in determining the vent geometry. To retain approximately the same percent of geometric openness as in the 40-ft unit, a vent diameter of 6.0 in. was required. It was also necessary to fold the radial tapes as they crossed the vent to reduce their cross section to 0.187 in. The distance between the centerline of adjacent radial tapes at the vent is therefore $6\pi/32$ or 0.59 in.

To ensure a longer parachute life during supersonic operation, it is essential to retain as much of the parent material flexibility as possible in all seams and joints. To preclude the radial tapes from overlapping as a result of unfavorable tolerance build-up, which would decrease flexibility in the vent area, the dimension between the radial tape centerlines at the vent was increased to 0.75 in. This increase is sufficient to permit the necessary lobing to occur between the radial tapes.

Four DGB parachutes, serial numbers 4, 5, 8, and 10, were equipped with a reefing system. The reefing line, 750-lb tensile strength, was attached to the leading edge of the disk by reefing rings located on each radial tape with the exception of two tapes where reefing line cutters were attached. The length of the reefing lines for each parachute are presented in Reference 5. The reefing line cutters, using a three-second time delay, were mechanically actuated by lanyard extraction at line stretch.

On the basis of recent subsonic wind tunnel testing at NASA/LRC, the disk reefing technique was established as being more satisfactory than reefing the leading- or trailing-edge of the band. As use of the parachute as a planetary entry device could necessitate reefed operation in either the subsonic or supersonic flow regimes, it appears most reasonable to use the above-mentioned technique for the current supersonic investigations.

DGB Stress Analysis

The DGB stress analysis considers a maximum decelerator load, based on the design requirements summarized in Section II. This load is calculated as follows.

$$F_o = C_{D_o} S_o q_\infty$$

$$= (1.0)(23.67)(70)$$

$$= 1663 \text{ lb.}$$

TABLE II - SUMMARY OF DGB CONSTRUCTED AND ACTUAL GEOMETRIC PROPERTIES

Geometric property	Serial number											
	1	2	3	4	5	6	7	8	9	10	11	12
λ_{g_D} (percent of S_o)	12.5	12.5	12.5	12.5	12.5	12.5	10.0	10.0	10.0	15.0	15.0	15.0
$\lambda_{g_{DB}}$ (percent of S_o)*	11.20	11.20	11.20	11.20	11.20	11.20	9.00	9.00	9.00	13.45	13.45	13.45
$\lambda_{g_{AB}}$ (percent of S_o)*	11.22	11.01	11.20	11.29	11.00	11.17	9.21	9.00	9.31	13.61	13.32	13.30
Nominal diameter, ft (design)	5.50	5.50	5.50	5.50	5.50	5.50	5.50	5.50	5.50	5.50	5.50	5.50
Nominal diameter, ft (actual)	5.39	5.41	5.39	5.38	5.41	5.37	5.39	5.45	5.39	5.41	5.47	5.43
Number of suspension lines	32	32	32	32	32	32	32	32	32	32	32	32
Length of suspension lines, ft (design)	5.50	5.50	5.50	5.50	5.50	5.50	5.50	5.50	5.50	5.50	5.50	5.50
Total area (S_o), sq in. (design)	3421	3421	3421	3421	3421	3421	3421	3421	3421	3421	3421	3421
Disk diameter, in. (design)	48.05	48.05	48.05	48.05	48.05	48.05	48.05	48.05	48.05	48.05	48.05	48.05
Disk area ($0.53 S_o$), sq in., (design)	1813	1813	1813	1813	1813	1813	1813	1813	1813	1813	1813	1813
Disk circumference, in. (design)	151.0	151.0	151.0	151.0	151.0	151.0	151.0	151.0	151.0	151.0	151.0	151.0
Vent diameter, in. (design)	6.00	6.00	6.00	6.00	6.00	6.00	6.00	6.00	6.00	6.00	6.00	6.00
Vent area ($0.0037 S_o$), sq in. (design)*	12.65	12.65	12.65	12.65	12.65	12.65	12.65	12.65	12.65	12.65	12.65	12.65
Vent area, sq in. (actual)*	11.44	11.62	11.36	11.50	11.78	11.39	12.00	11.55	11.48	11.91	11.81	11.87
Gap width, in. (design)	2.749	2.749	2.749	2.749	2.749	2.749	2.183	2.183	2.183	3.316	3.316	3.316
Gap area ($0.1213 S_o$), sq in., (design)	415.0	415.0	415.0	415.0	415.0	415.0	329.5	329.5	329.5	500.5	500.5	500.5
Gap area, sq in. (actual)*	356.0	356.0	356.0	361.0	349.0	351.0	288.0	290.0	295.0	441.0	435.0	432.0
Band width, in. (design)	7.903	7.093	7.093	7.903	7.093	7.903	8.467	8.467	8.467	7.337	7.337	7.337
Band area, sq in. (design)	1193	1193	1193	1193	1193	1193	1279	1279	1279	1108	1108	1108

*Blockage by radial tapes accounted for.

On the basis of Reference 8, safety factors ranging in value from 1.5 to 2.0 are generally recommended for design of parachutes intended for flight application. However, experience has indicated that a more conservative value of 3.0 provides additional assurance of a reasonable operational life during wind-tunnel testing. The safety factor of 3.0 has been used in the subsequent analysis. A summary of the strength loss and safety factors which establish the overall design factors used in the DGB stress analysis is presented in Table III.

TABLE III - STRENGTH-LOSS AND SAFETY FACTORS (DGB PARACHUTE)

Symbol	Factor	Main seams	Radial tape	Suspension lines	Reinforcement bands
m	Joint efficiency	0.80	0.80	0.80	0.80
e	Abrasion	0.95	0.95	0.95	0.95
j	Safety	3.00	3.00	3.00	3.00
c	Line convergence	. . .	1.05	1.05	. . .
f	Asymmetrical loading	1.05	1.05	1.05	1.05
$\frac{jcf}{me}$	Design	4.15	4.35	4.35	4.15

The following analyses demonstrate the DGB design adequacy on the basis of the method utilized in the design of the DGB parachutes (Reference 7) tested during the PEPP and SPED-I flight test programs.

The load developed in the suspension lines and radial tapes is

$$\begin{aligned}
 P_{\text{dev}} &= \frac{F_o}{Z} \\
 &= \frac{1663}{32} \\
 &= 52.0 \text{ lb.}
 \end{aligned}$$

Using the appropriate design factor from Table III, the allowable load in the suspension lines, which have a 300-lb ultimate tensile strength, is

$$\begin{aligned}
 P_{\text{all}} &= \frac{P_{\text{dev}}}{4.35} \\
 &= \frac{300}{4.35} \\
 &= 70.5 \text{ lb.}
 \end{aligned}$$

The allowable load in the radial tapes, which have a 350-lb ultimate tensile strength, is

$$\begin{aligned} P_{\text{all}} &= \frac{350}{4.35} \\ &= 80.5. \end{aligned}$$

The margin of safety for the suspension lines is

$$\begin{aligned} \text{M. S.} &= \frac{P_{\text{all}}}{P_{\text{dev}}} - 1.0 \\ &= \left(\frac{70.5}{52.0} \right) - 1.0 \\ &= 0.36. \end{aligned}$$

The margin of safety for the radials is

$$\begin{aligned} \text{M. S.} &= \left(\frac{80.5}{52.0} \right) - 1.0 \\ &= 0.55. \end{aligned}$$

The horizontal component of the suspension line load is calculated from the geometry of Figure 2 as follows:

$$\begin{aligned} P_H &= P_{sl} \left(\frac{1.83}{5.5} \right) \\ &= 52 \left(\frac{1.83}{5.5} \right) \\ &= 17.3 \text{ lb.} \end{aligned}$$

The radius of the band and leading edge of the disk gore lobe, assumed equal for purposes of analysis, can be calculated from the geometry of Figure 3 as follows.

From the ratio $l/c = 1.095$,

$$2\theta = 84 \text{ deg, or } \theta = 42 \text{ deg ;}$$

and from the relation $r_l = c/2 \sin \theta$,

$$\begin{aligned} r_l &= \frac{4.25}{(2)(0.67)} \\ &= 3.18 \text{ in.} \end{aligned}$$

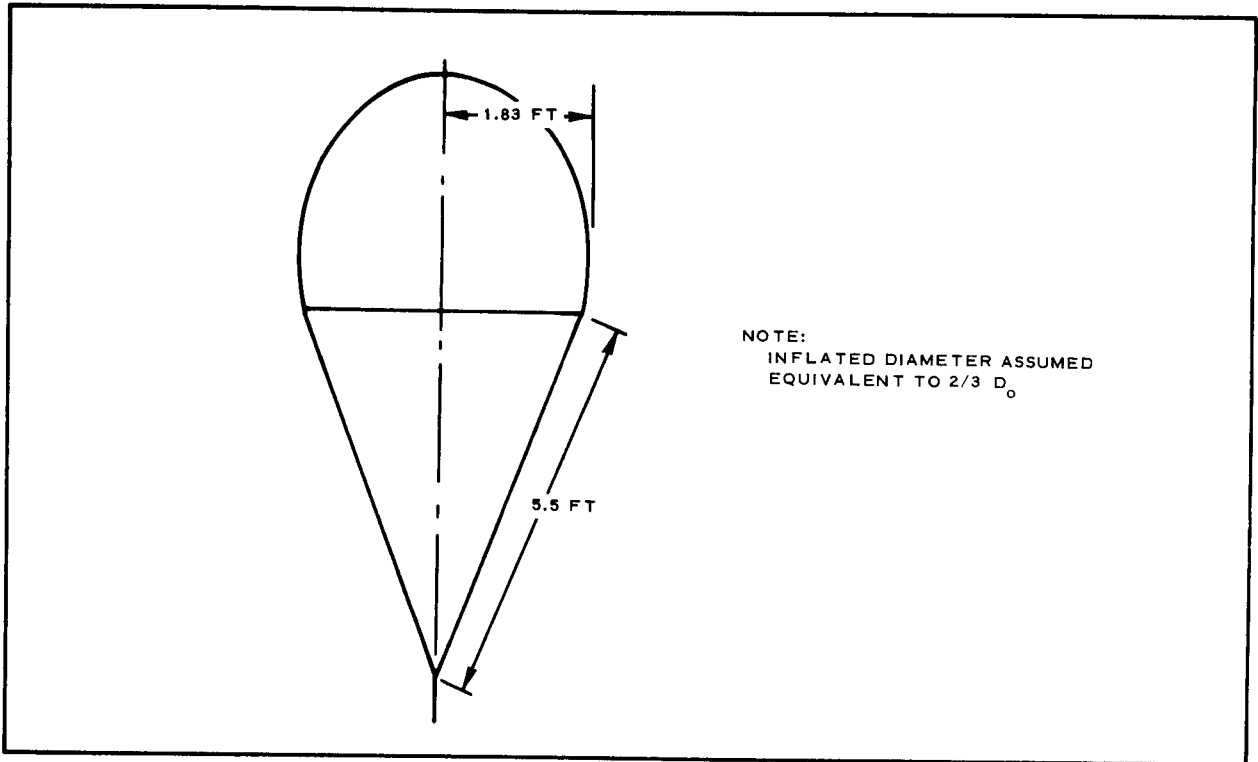


Figure 2 - DGB Inflated Geometry

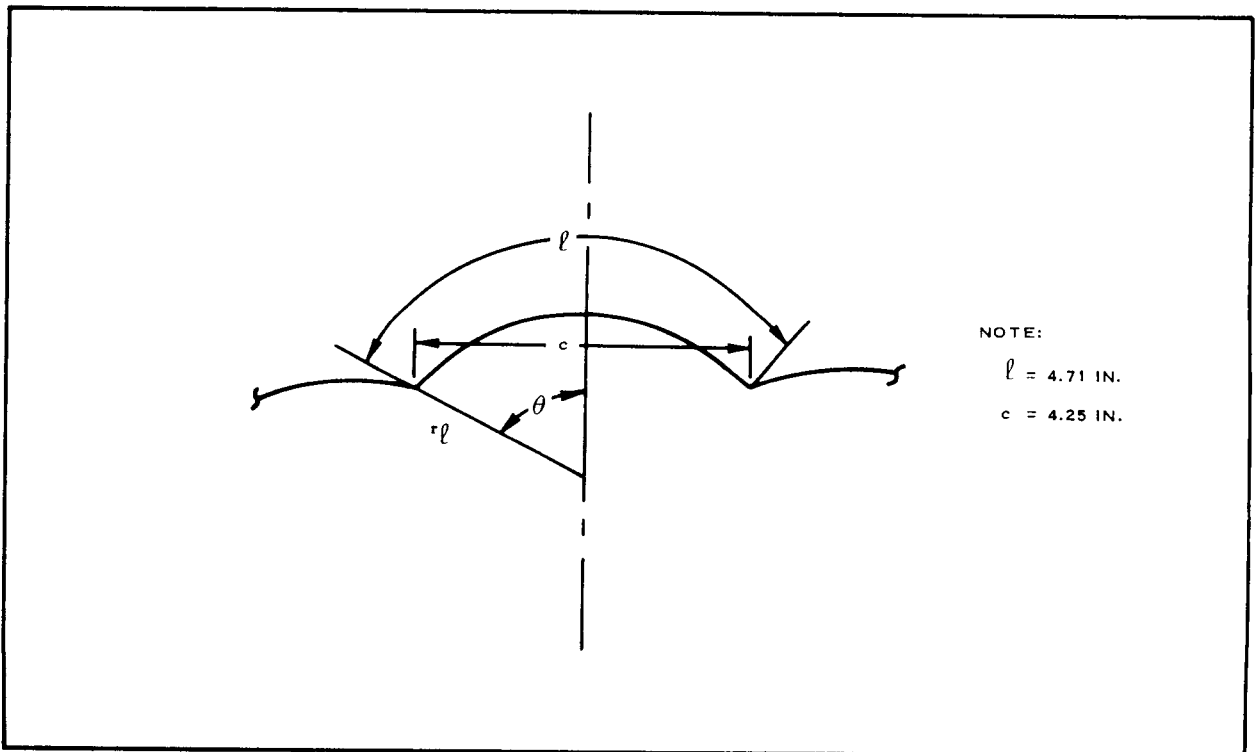


Figure 3 - Cross-Section of Band Gore Lobe

The load developed in the band and leading edge of the disk reinforcement bands can be calculated from the geometry of Figure 4 as follows:

$$\begin{aligned}
 P_{\text{dev}} &= P_{\text{sb}} \\
 &= \left(\frac{P_{\text{H}}}{Z} \right) \left(\frac{\ell}{\cos \gamma} \right) \\
 &= \left(\frac{17.30}{2} \right) \left(\frac{1}{0.59} \right) \\
 &= 14.7 \text{ lb.}
 \end{aligned}$$

The allowable load in the reinforcement tapes, which have a 350-lb ultimate tensile strength, is

$$\begin{aligned}
 P_{\text{all}} &= \frac{350}{4.15} \\
 &= 84.4 \text{ lb.}
 \end{aligned}$$

The margin of safety for the reinforcement tapes is

$$\begin{aligned}
 \text{M. S.} &= \left(\frac{84.4}{14.7} \right) - 1.0 \\
 &= 7.47.
 \end{aligned}$$

From the geometry of Figure 5, the angle subtending the gore width at the vent is

$$\begin{aligned}
 2\alpha &= \frac{360 \text{ deg}}{Z} \\
 &= 11.250 \text{ deg}
 \end{aligned}$$

or,

$$\alpha = 5.625 \text{ deg.}$$

The vent tape reinforcement length between radial tapes is 0.75 in. while the cord length based on the vent diameter is 0.59 in. From the ratio of $0.75/0.59 = 1.27$, the included angle between radial tapes of the lobe radius is found to be 135 deg.

From the geometry of Figure 6, the load developed in the vent reinforcement tape can be determined as follows:

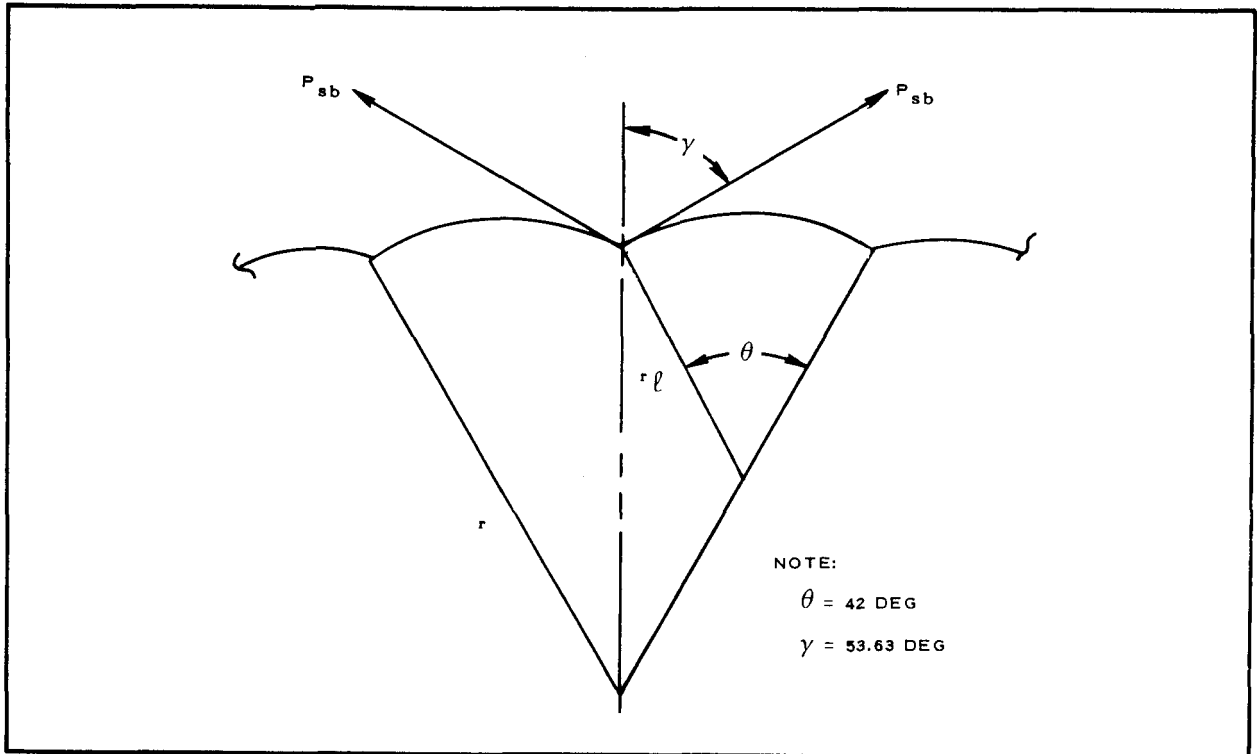


Figure 4 - Free-Body Diagram of Band and Disk Reinforcement Band

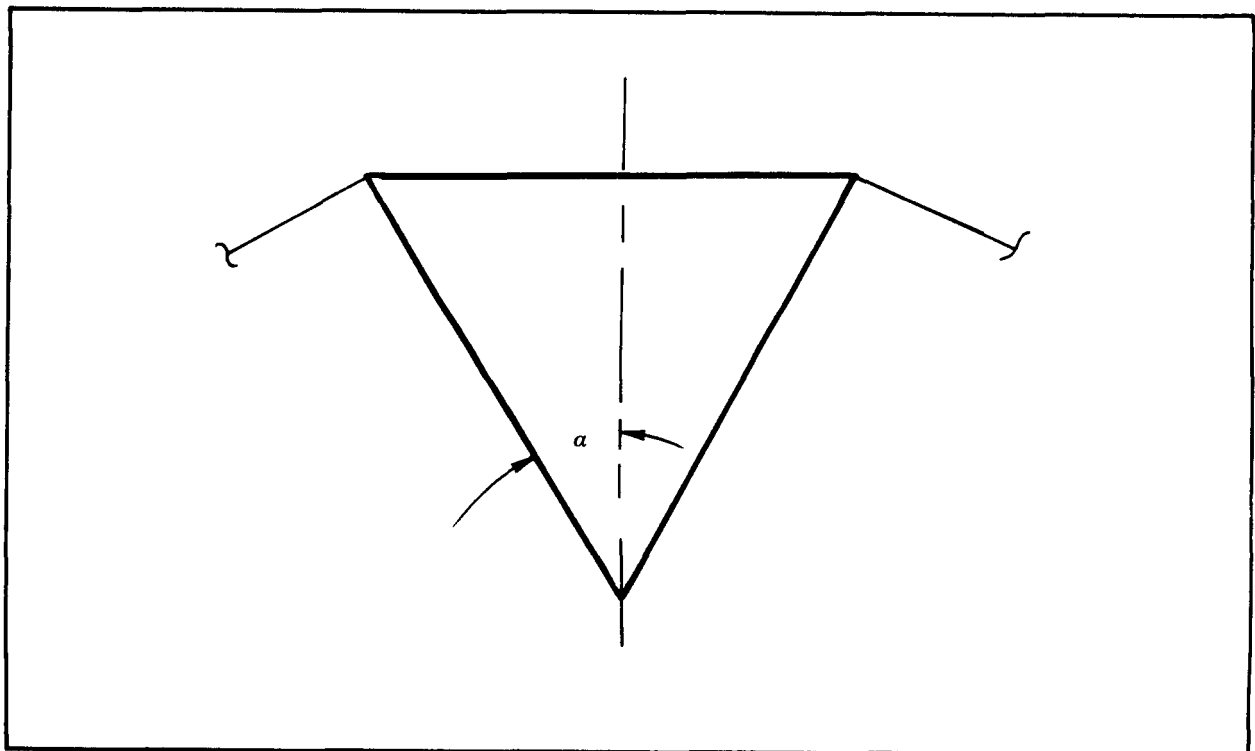


Figure 5 - Vent Geometry

The load developed in the canopy cloth, worst case considered to be when F_o is absorbed by the disk area, (assuming the inflated disk and band diameter^o are equal to $2 D_o/3$) is

$$\begin{aligned} P_{\text{dev}} &= \frac{F_o}{S_D} R_{PD} \\ &= \left(\frac{1663}{1813} \right) (22.0) \\ &= 20.2 \text{ lb/in.} \end{aligned}$$

The allowable load in the canopy cloth which has an 80 lb/in.^a ultimate limit is

$$\begin{aligned} P_{\text{all}} &= \frac{80}{3.82} \\ &= 21.0 \text{ lb/in.,} \end{aligned}$$

where the joint efficiency is equal to one. The margin of safety in the canopy cloth is

$$\begin{aligned} \text{M. S.} &= \left(\frac{21.0}{20.2} \right) - 1.0 \\ &= 0.04 \text{ (ignoring gore lobing).} \end{aligned}$$

The load developed in the vent radials, worst case considered to be when F_o is carried by radials, is

$$\begin{aligned} P_{\text{dev}} &= \frac{1663}{32} \\ &= 52.0 \text{ lb.} \end{aligned}$$

The allowable load in the vent radials, which have a 350-lb ultimate tensile strength, is

$$\begin{aligned} P_{\text{all}} &= \frac{350}{2.0} \\ &= 175 \text{ lb,} \end{aligned}$$

where $F_d = 2.0$ is used as a flutter factor.

The margin of safety is

$$\begin{aligned} \text{M. S.} &= \left(\frac{175}{52} \right) - 1.0 \\ &= 2.36. \end{aligned}$$

^aRated strength.

The load developed in the disk main seam, worst case considered to be when F_o is absorbed by the disk area, is

$$\begin{aligned}P_{\text{dev}} &= \left(\frac{F_o}{S_D}\right) R_{P_D} \\&= \left(\frac{1663}{1813}\right) 22.0 \\&= 20.2 \text{ lb/in.}\end{aligned}$$

The allowable load, using the minimum strip tensile strength of the canopy cloth, is

$$\begin{aligned}P_{\text{all}} &= \frac{80}{4.15} \\&= 19.3 \text{ lb/in.}\end{aligned}$$

The margin of safety is

$$\begin{aligned}\text{M.S.} &= \frac{19.3}{20.2} - 1.0 \\&= -0.04 \text{ (ignoring gore lobe).}^a\end{aligned}$$

The load developed in the band main seam, worst case considered to be when F_o is absorbed uniformly by the total canopy, is

$$\begin{aligned}P_{\text{dev}} &= \left(\frac{F_o}{S_o}\right) R_{P_D} \\&= \left(\frac{1663}{3421}\right) (22.0) \\&= 10.70 \text{ lb/in.}\end{aligned}$$

The allowable load, using the minimum strip tensile strength of the canopy cloth, is

$$\begin{aligned}P_{\text{all}} &= \frac{80}{4.15} \\&= 19.3 \text{ lb/in.}\end{aligned}$$

The margin of safety is

^aThe margin based on the cloth strength determined by static test (84 lb/in. - min) is 0.0.

$$\begin{aligned} \text{M.S.} &= \left(\frac{19.3}{10.7} \right) - 1.0 \\ &= 0.80. \end{aligned}$$

From the geometry of Figure 7, the load developed in the disk cross seam is

$$\begin{aligned} P_{\text{dev}} &= \left(P_{\text{dev}_r} \right) (\sin \alpha) \\ &= (20.2)(0.707) \\ &= 14.3 \text{ lb/in.} \end{aligned}$$

The allowable load is

$$\begin{aligned} P_{\text{all}} &= \frac{80}{4.15} \\ &= 19.3 \text{ lb/in.} \end{aligned}$$

The margin of safety is

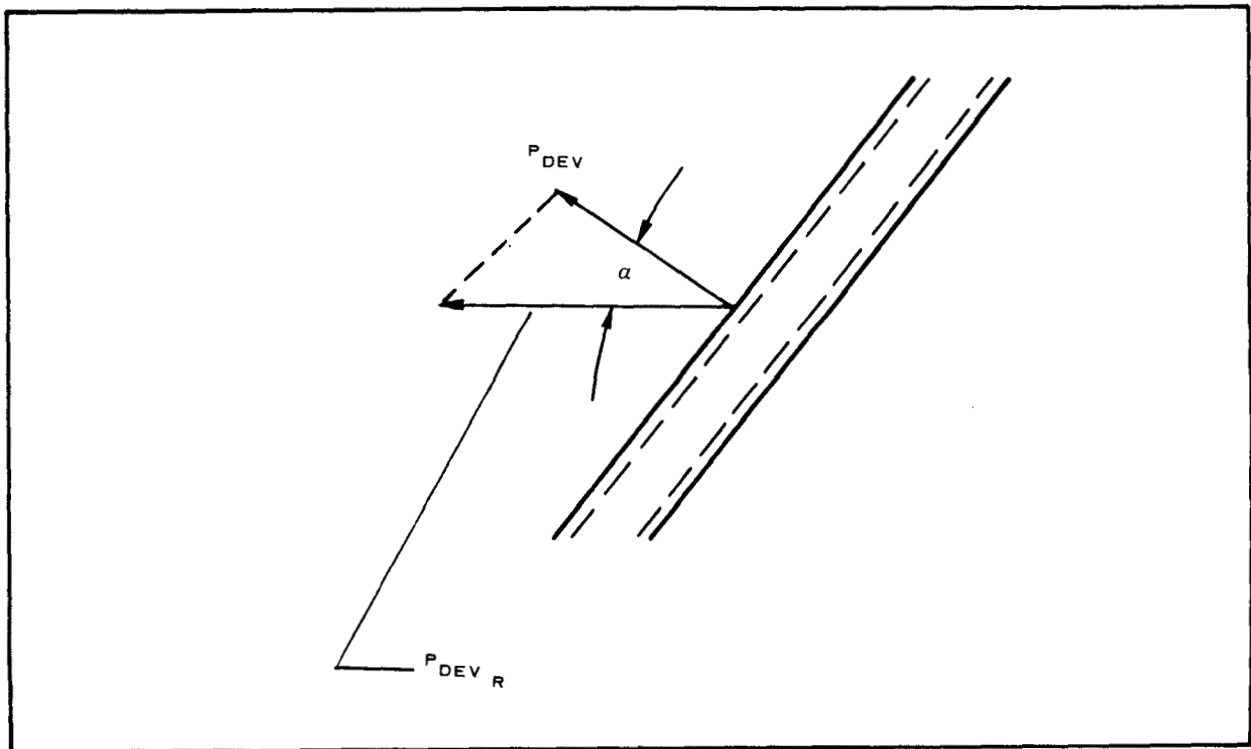


Figure 7 - Disk Gore Cross Seam

$$\begin{aligned} \text{M. S.} &= \left(\frac{19.3}{14.3} \right) - 1.0 \\ &= 0.35. \end{aligned}$$

The load developed in the band cross seam is

$$\begin{aligned} P_{\text{dev}} &= \left(\frac{F_o}{S_o} \right) (R_{p_D}) (\sin \alpha) \\ &= \left(\frac{1663}{3421} \right) (22.0)(0.707) \\ &= 7.56 \text{ lb/in.} \end{aligned}$$

The allowable load is

$$\begin{aligned} P_{\text{all}} &= \frac{80}{4.15} \\ &= 19.3 \text{ lb/in.} \end{aligned}$$

The margin of safety is

$$\begin{aligned} \text{M. S.} &= \left(\frac{19.3}{7.56} \right) - 1.0 \\ &= 1.55. \end{aligned}$$

Ringsail Gore Pattern and Design Data

The method of Reference 9 was used to establish the basic parachute gore pattern except where consideration of scale and possible buildup of fabrication tolerances dictated variations.

The use of 54 gores and 10 rings and sails, as used in the 55-ft ringsail flight-tested by NASA/LRC, was not possible in the 5.5-ft model for this program. This is primarily a result of the material requirements not scaling, because of a factor of seven difference in the operating dynamic pressure. The use of 30 gores and 5 rings and sails for the parachute was based on retaining, to the extent possible, the geometric proportions of the 55-ft diameter parachute. The appropriate ringsail parameters then were applied to determine the diameter of the sphere on whose surface the required canopy area subtended a 108-deg vertex angle (see Figure 8).

Ringsail parachutes present problems arising from infolding at the skirt as a result of the excess material required for fullness. To eliminate this excess and minimize infolding, the canopy nominal area was increased by the factor 1.074 and the sphere diameter was recalculated accordingly. The gore

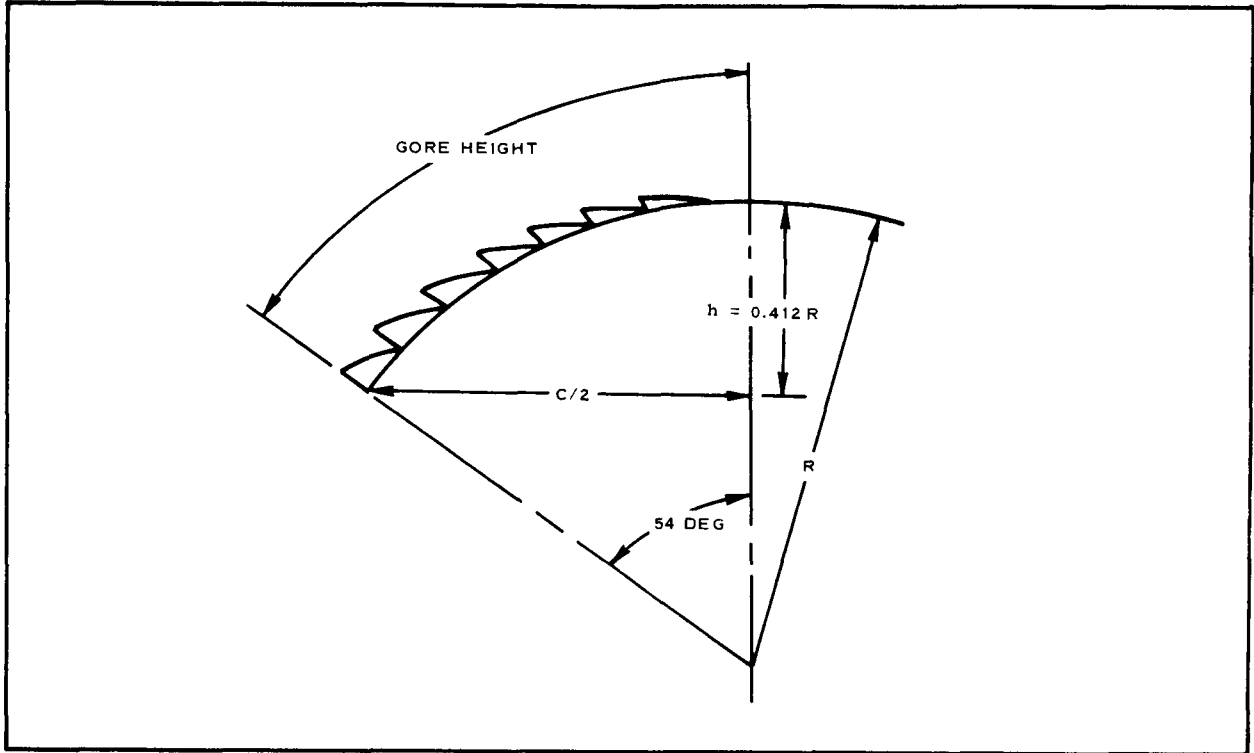


Figure 8 - Basic Ringsail Geometry

parameters then were calculated as if the parachute had the larger area. However, to retain the proper canopy area, only 30 gores were assigned to the parachute. Thus, the area used to calculate the radius of the sphere was

$$\begin{aligned} A &= (23.76)(1.074) \\ &= 25.52 \text{ sq ft} \end{aligned}$$

From the geometry of Figure 8,

$$\begin{aligned} A &= 2\pi Rh \\ &= 25.52 \text{ sq ft} \end{aligned}$$

and

$$h = 0.412 R.$$

Therefore,

$$\begin{aligned} A &= 2\pi R(0.412 R) \\ &= 0.824\pi R^2, \end{aligned}$$

or

$$R = \left(\frac{25.52}{0.824\pi} \right)^{1/2}$$

$$= 3.140 \text{ ft.}$$

The total gore height is

$$H_g = (3.140)(12)(54) \left(\frac{\pi}{180} \right)$$

$$= 35.509 \text{ in.}$$

The method used to calculate the basic gore dimensions and the results of these calculations are summarized in Figure 9.

Of the five sails, the upper two were actually rings separated by 0.25-in. slots. To achieve the desired geometric porosity, there was an opening above the fifth sail. Calculation of the gore widths at all necessary points was possible, by linear interpolation between the closest two values of Figure 9, since the distance up the center of the gore was known for the leading and trailing edges of each sail and ring.

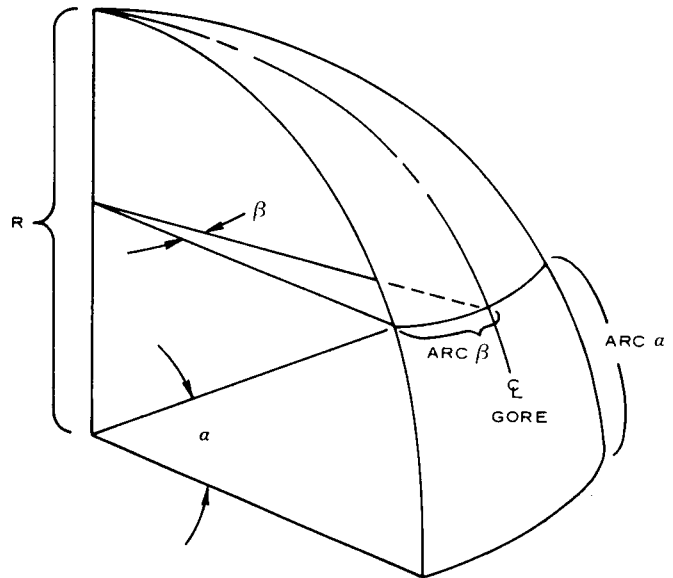
After the basic ring and sail dimensions were calculated, fullness was added. The basic ring and sail dimensions, with and without fullness, are shown in Table IV, and the fullness added is presented in Figure 10.

Next, the ring and sail pattern dimensions, including seam allowances were calculated. The final pattern dimensions are summarized in Figure 11.

TABLE IV - SAIL DIMENSIONS FOR THE 5.5-FT RINGSAIL

Sail no.	Position	Distance along gore (in.)	Width without fullness (in.)	Fullness (percent)	Width with fullness (in.)
1	Top	33	0.4888	2.0	1/2
	Bottom	27	1.6423	2.0	1-11/16
2	Top	26-3/4	1.6898	2.0	1-23/32
	Bottom	20-3/4	2.7994	2.0	2-27/32
3	Top	20-1/2	2.8444	2.0	2-29/32
	Bottom	14-1/2	3.8802	3.5	4-1/32
4	Top	14-1/2	3.8802	1.0	3-29/32
	Bottom	8-7/16	4.8194	5.5	5-3/32
5	Top	6-1/16	5.1780	0.0	5-3/16
	Bottom	0	5.9376	7.5	5-25/32

$$\begin{aligned}
 R &= 3.1397 \text{ FT} \\
 &= 37.6762 \text{ IN.} \\
 \beta &= \frac{360}{2(30)(1.0741)} = 5.5807 \text{ DEG} \\
 &= 0.09740 \text{ RAD}
 \end{aligned}$$



α (DEG)	$\cos \alpha$	α (RAD)	ARC α (IN.) [*]	ARC α - 23.6720 (IN.)	ARC β (IN.) [†]	2 ARC β (IN.)
90.0	0.0000	1.5708	59.1816	35.5096	0.0000	0.0000
86.2	0.0666	1.5042	56.6720	33.0000	0.2444	0.4888
85.0	0.0872	1.4835	55.8927	32.2207	0.3200	0.6400
80.0	0.1737	1.3963	52.6073	28.9353	0.6374	1.2748
75.0	0.2588	1.3090	49.3182	25.6462	0.9497	1.8994
70.0	0.3420	1.2217	46.0290	22.3570	1.2550	2.5100
65.0	0.4226	1.1345	42.7437	19.0717	1.5508	3.1016
60.0	0.5000	1.0472	39.4545	15.7825	1.8348	3.6696
55.0	0.5736	0.9599	36.1654	12.4934	2.1049	4.2098
50.0	0.6428	0.8727	32.8800	9.2080	2.3589	4.7178
45.0	0.7071	0.7854	29.5909	5.9189	2.5948	5.1896
40.0	0.7660	0.6981	26.3720	2.6298	2.8110	5.6220
36.0	0.8090	0.6283	23.6720	0.0000	2.9688	5.9376

^{*} ARC α = $R\alpha$, WHERE R IS IN INCHES AND α IS IN RADIAN.

[†] ARC β = $R\beta \cos \alpha$, WHERE R IS IN INCHES AND β IS IN RADIAN.

Figure 9 - Basic Gore Dimensions for the 5.5-Ft Ringsail

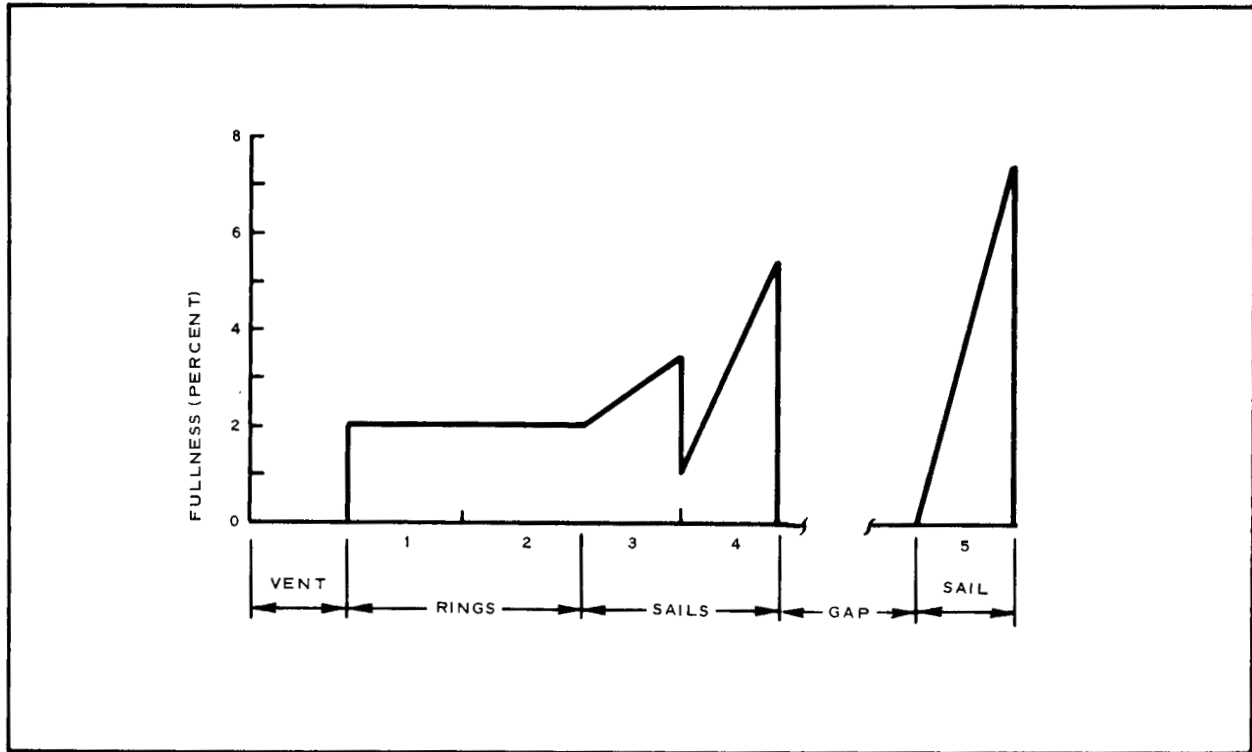


Figure 10 - Fullness Added to 5.5-Ft Ringsail

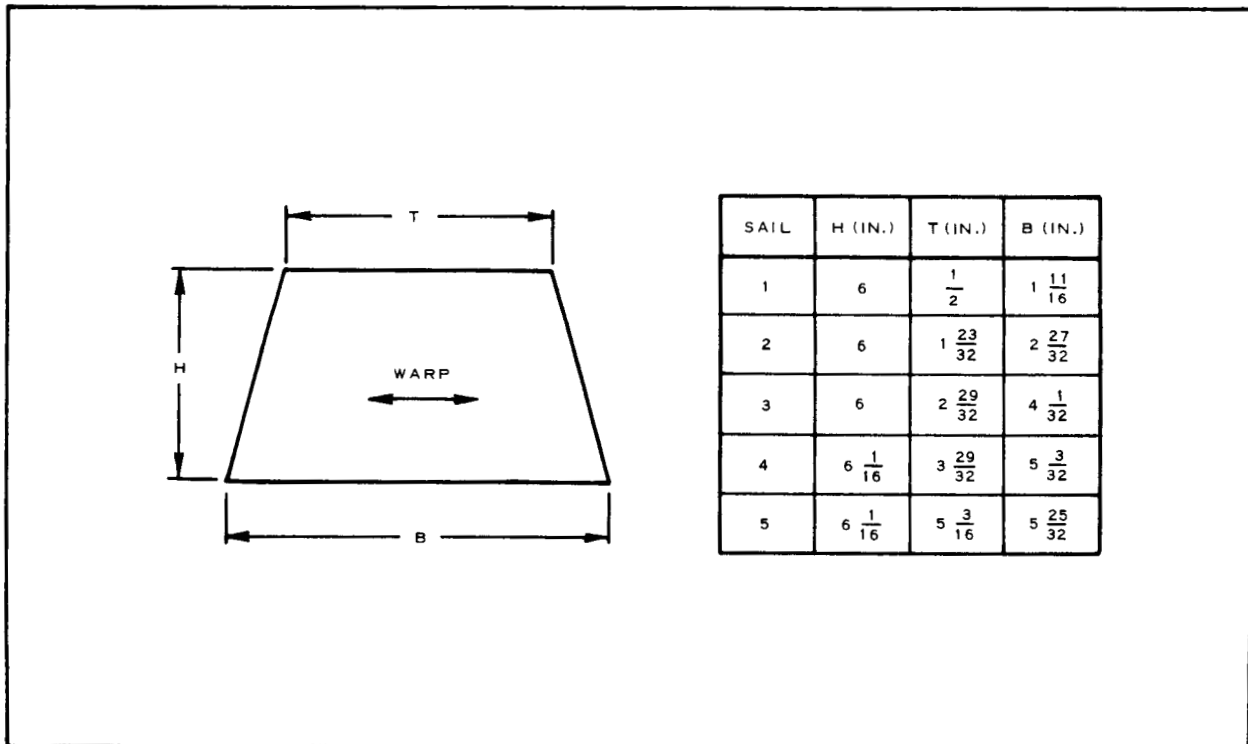


Figure 11 - Ring and Sail Patterns for the 5.5-Ft Ringsail

Due to the manner in which the ringsail geometric porosity is achieved (as contrasted to the vent and single gap of the DGB), it is inherently more susceptible to variations in geometric porosity as a result of fabrication tolerances. These variations will be, in terms of percent of change in geometric porosity, more significant in the case of the wind-tunnel models than the large flight models. The reason for the increased significance in the case of the wind-tunnel models results from the fact that fabrication tolerances are essentially independent of scale. Although rigid fabrication tolerances were maintained, it may be shown that variations in geometric porosity of ± 2.25 percent (in terms of percent of nominal surface area) could exist.

The above discussion has relevance in view of the requirement that the ringsail parachute have a geometric porosity of 15 percent. There is evidence, Reference 2, that the 15-percent geometric porosity value is approaching a limit with respect to canopy inflation stability over the intended Mach number range of operation. Figure 10 of Reference 2, which is reproduced in Figure 12 below, indicates that a value of 15 percent is marginal at Mach 2.6. Reference 2 notes that the parachute tested at $M = 2.7$ is on the border of the region of inflation instability, and the significant changes in projected area of the canopy are apparently a result of this instability.

In view of the above discussion of inflation instability and fabrication tolerances, the ringsail parachute was designed to have a geometric porosity of 12.75 percent since a design value of 15 percent could result in an actual value as high as 17.25 percent.

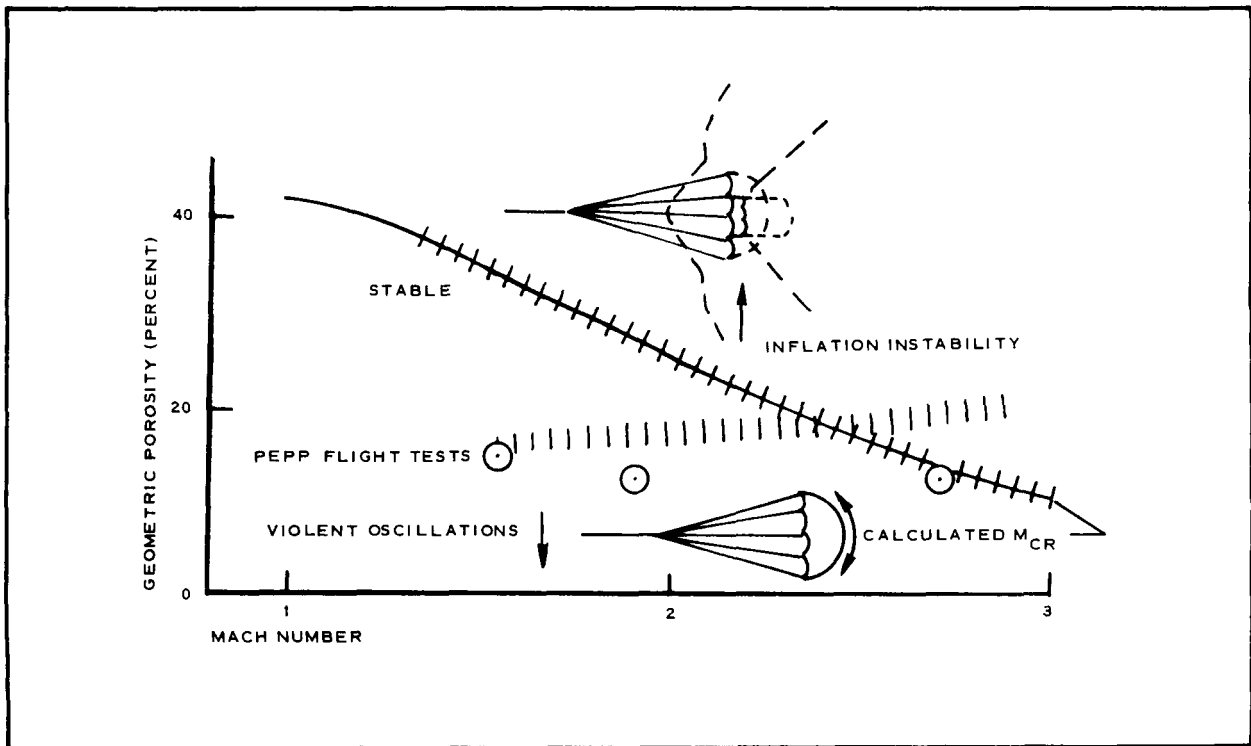


Figure 12 - Parachute Stability Regions

The procedure used to calculate the geometric porosity consisted of determining the total area of a single gore from the basic gore dimensions calculated by the previously discussed method and comparing that area with the total open area of the gore (referenced method accounts for radial tape blockage).

In determining the gore total area, it was assumed that a gore is composed of a number of trapezoids with a terminal triangle at the vent end. Figure 13 illustrates how this assumption was applied to the 5.5-ft nominal diameter parachute. All dimensions shown in the figure result from the previously discussed gore geometry calculation procedure.

The open area was calculated after the number and size of the rings and sails and the amount of fullness added to the sails was determined. The open area was considered to consist of the following items:

1. Vent
2. Slots in the crown area (assumed trapezoidal)
3. Gap above the bottom sail (assumed trapezoidal and surmounted by a sail scoop)
4. Sail scoops (assumed to be triangles)

In the inflated condition, the sail scoops may at any given time resemble anything from a thin crescent (considered to be most probable) to an ellipse. On the basis of the references method, 75 percent of the triangular shape was taken as a reasonable approximation for purposes of porosity calculations. Possible shapes, including the assumed shape are shown in Figure 14.

The total area of one gore, calculated from the geometry of Figure 14, is

$$\begin{aligned} \frac{S_o}{Z} &= (2.6298 \times 5.7798) + 3.2891(5.4058 + 4.9537 + 3.9397 + 1.5871) + \\ &\quad 3.2854(4.4638 + 0.9574) + 3.2892(3.3856 + 2.2047) + \\ &\quad (3.2853 \times 2.8058) + (0.7793 \times 0.5644) + (2.5096 \times 0.2444) \\ &= 113.9207 \text{ sq in.} \end{aligned}$$

The total open area of one gore is calculated as follows.

The vent open area (less radial blockage),

$$\begin{aligned} S_v &= 0.5 (\text{base-radial blockage})(\text{alt} - \text{radial blockage}) \\ &= 0.5(0.4888 - 0.2000)(2.5096 - 1.0277) \\ &= 0.2140 \text{ sq in.} \end{aligned}$$

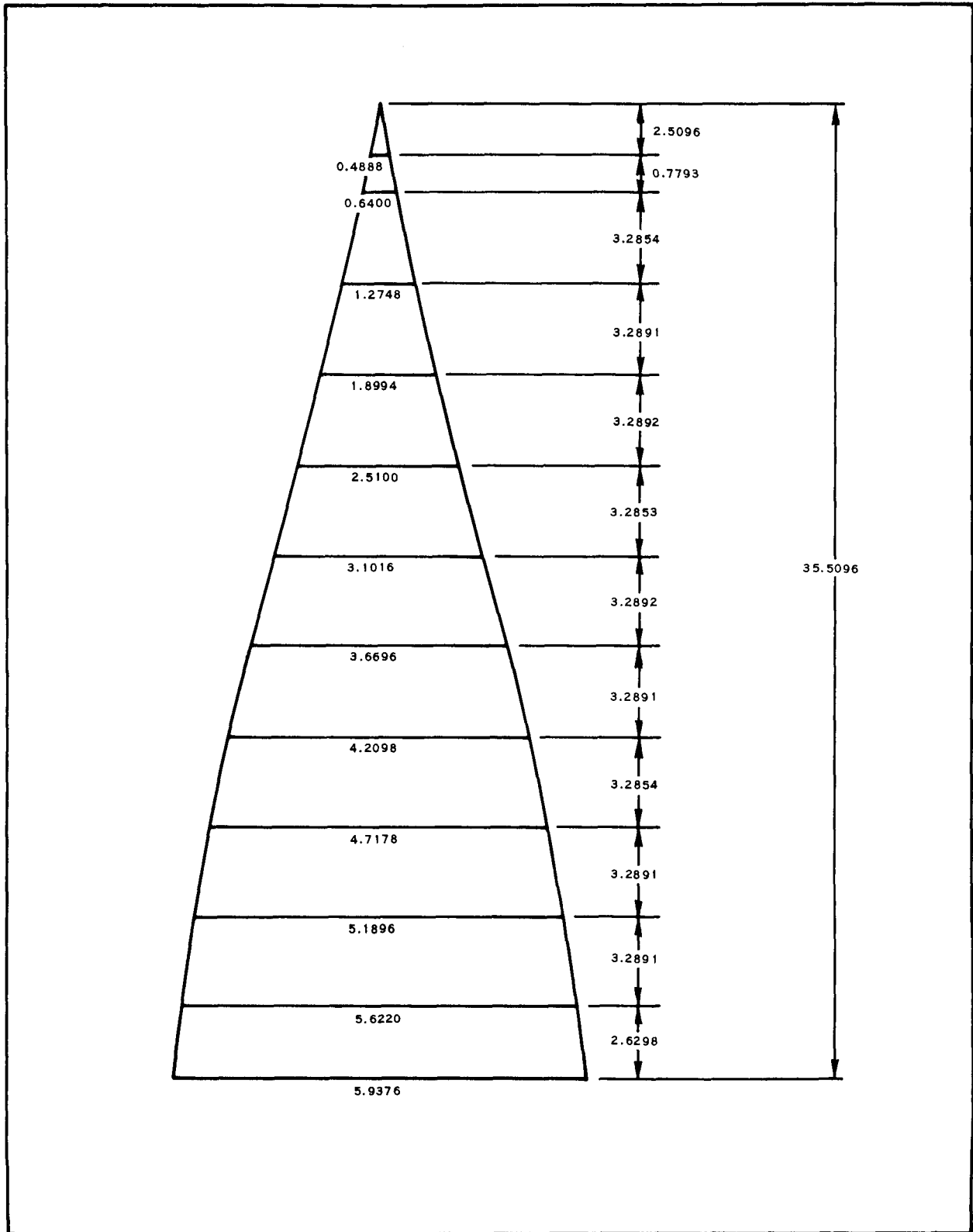


Figure 13 - Basic Gore of the 5.5-Ft Ringsail

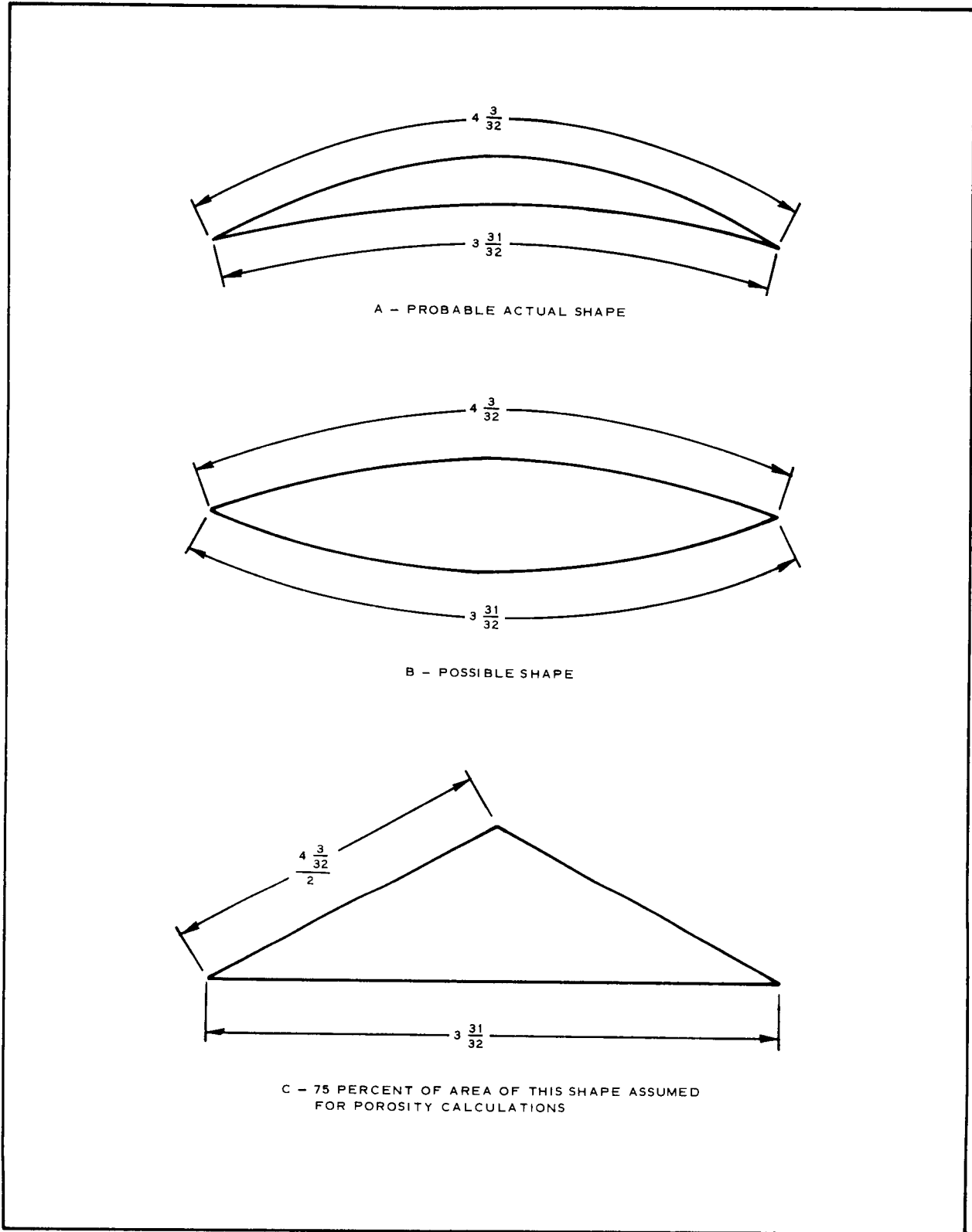


Figure 14 - Scoop Shape

The slot area (less radial blockage),

$$\begin{aligned} S_s &= 0.25 \left[(1.7656 - 0.500) + (2.9375 - 0.500) \right] \\ &= 0.9258 \text{ sq in.} \end{aligned}$$

Therefore, the crown-area geometric porosity is

$$\begin{aligned} \lambda_{g_c} &= \frac{(S_v + S_s)(100)}{\frac{S_o}{Z}} \\ &= \frac{(0.2140 + 0.9258)(100)}{113.9207} \\ &= 1.00 \text{ percent.} \end{aligned}$$

The gap area (less radial blockage), calculated from the geometry of Figure 15 is

$$\begin{aligned} S_g &= (2.375)(0.5)(5.000 + 4.3819) + 0.75(2.1909)(0.7874) \\ &= 12.7027 \text{ sq in.} \end{aligned}$$

The sail scoop area (less radial blockage) calculated from the geometry of Figure 16 is

$$\begin{aligned} S_{ss} &= 0.75(1.7349)(0.4698) \\ &= 0.6111 \text{ sq in.} \end{aligned}$$

The total open area of one gore is

$$\begin{aligned} S_{\text{open}} &= 0.2140 + 0.9250 + 12.7027 + 0.6111 \\ &= 14.4528 \text{ sq in.} \end{aligned}$$

Hence, the total geometric porosity, in percent of the nominal surface area, is

$$\begin{aligned} \lambda_g &= \frac{(14.4528)(100)}{113.9207} \\ &= 12.81 \text{ percent.} \end{aligned}$$

The 12.81 percent value is considered sufficiently close to the desired 12.75 percent in view of tolerance variations and the necessary assumption involving the scale scoop shape.

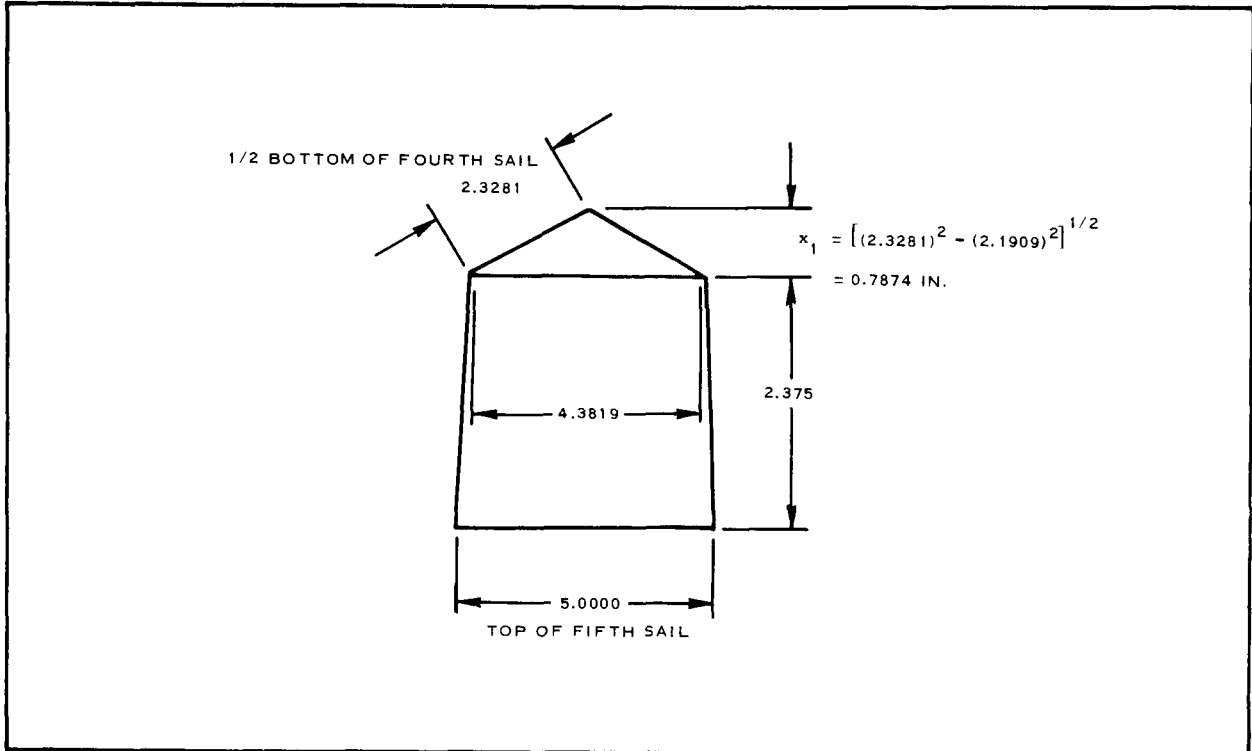


Figure 15 - Geometry of Gap

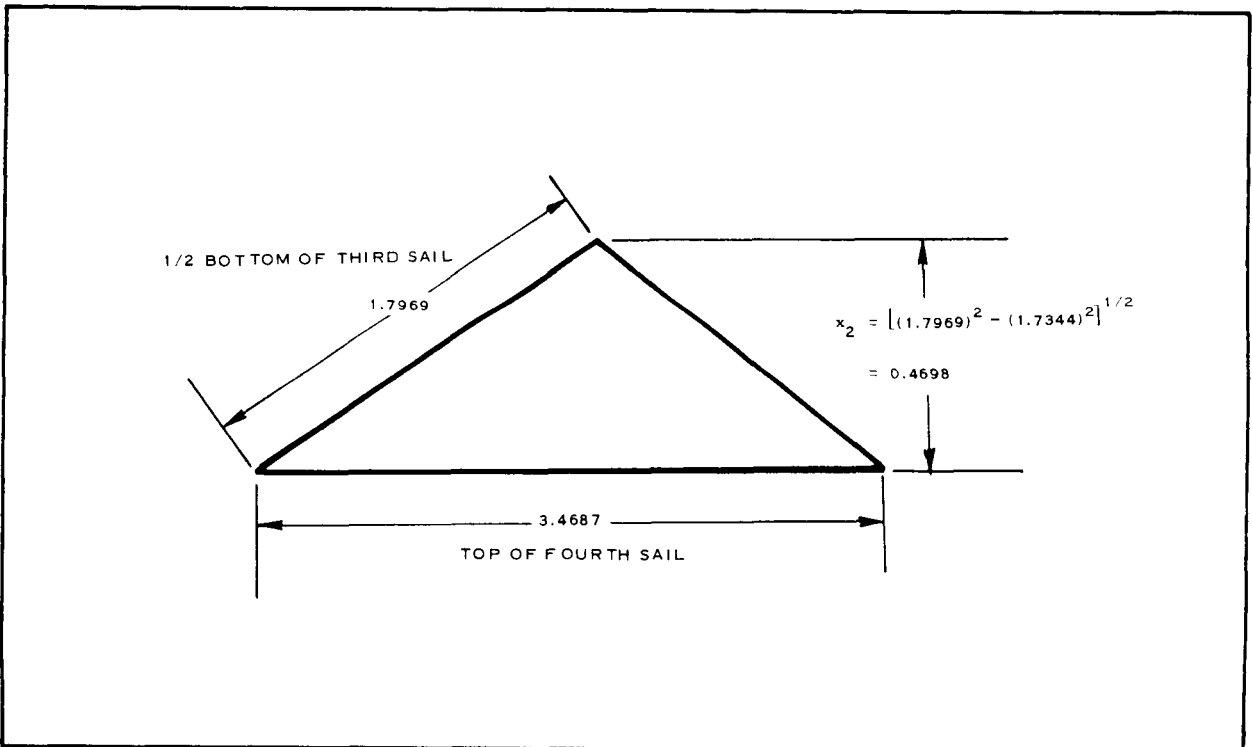


Figure 16 - Geometry of Sail Scoop

Ringsail Stress Analysis

As in the case of the DGB, the maximum decelerator load, based on the design requirements summarized in Section II, is

$$\begin{aligned}F_o &= C_{D_o} S_o q_\infty \\ &= (1.0)(23.67)(70) \\ &= 1663 \text{ lb.}\end{aligned}$$

The following analysis demonstrates the ringsail design adequacy on the basis of methods used in the design of the 55-ft ringsail parachute (Reference 9) tested during the PEPP flight-test program.

The load developed in the suspension lines and radial tapes is

$$\begin{aligned}P_{\text{dev}} &= \frac{F_o}{Z} \\ &= \frac{1663}{30} \\ &= 55.5 \text{ lb.}\end{aligned}$$

Using the appropriate design factor (see Table V), the allowable load in suspension lines which have a 300-lb ultimate tensile strength is

$$\begin{aligned}P_{\text{all}} &= \frac{300}{4.35} \\ &= 70.5\end{aligned}$$

The allowable load in the radial tapes, which have a 350-lb ultimate tensile strength is

$$\begin{aligned}P_{\text{all}} &= \frac{350}{4.35} \\ &= 80.5\end{aligned}$$

The margin of safety for the suspension lines is

$$\begin{aligned}\text{M. S.} &= \left(\frac{P_{\text{all}}}{P_{\text{dev}}} \right) - 1.0 \\ &= \left(\frac{70.5}{55.5} \right) - 1.0 \\ &= 0.245,\end{aligned}$$

TABLE V - STRENGTH-LOSS AND SAFETY FACTORS
(RINGSAIL PARACHUTE)

Symbol	Factor	Main seams, rings, and sails	Radial tape	Suspension lines	Vent and skirt reinforcement band
m	Joint efficiency	0.80	0.80	0.80	0.80
e	Abrasion	0.95	0.95	0.95	0.95
j	Safety	3.00	3.00	3.00	3.00
c	Line convergence	. . .	1.05	1.05	. . .
f	Asymmetrical loading	1.05	1.05	1.05	1.05
$\frac{jcf}{me}$	Design	4.15	4.35	4.35	4.15

and the margin of safety for the radials is

$$\begin{aligned}
 \text{M.S.} &= \frac{80.5}{55.5} - 1.0 \\
 &= 1.45 - 1.0 \\
 &= 0.45.
 \end{aligned}$$

The load developed in the canopy cloth is determined through the following procedure:

1. The diameter of the inflated canopy is assumed to be $0.67 D_0$ or 3.68 ft, which corresponds to a projected area of 10.65 sq ft.
2. The maximum decelerator load, 1663 lb, is divided by the projected area of the canopy, yielding a pressure differential of 1.09 psi.
3. The load developed in pounds per inch is

$$\begin{aligned}
 P_{\text{dev}} &= \frac{PR}{2} \text{ (sails and rings assumed taut in the inflated condition)} \\
 &= (1.09) \left(\frac{22.1}{2} \right) \\
 &= 12.0 \text{ lb/in.}
 \end{aligned}$$

The allowable load in the canopy cloth, which has an 80-lb/in. ultimate tensile strength, is

$$\begin{aligned}P_{\text{all}} &= \frac{80}{3.82} \\ &= 21.0 \text{ lb/in.}\end{aligned}$$

where the joint efficiency is equal to one. The margin of safety for the canopy cloth is

$$\begin{aligned}\text{M. S.} &= \left(\frac{21.0}{12.0}\right) - 1.0 \\ &= 0.74.\end{aligned}$$

The horizontal component of the suspension line load is calculated from the geometry of Figure 17 as follows:

$$\begin{aligned}P_{\text{H}} &= P_{\text{s}} \left(\frac{1.83}{6.5}\right) \\ &= 55.5 \left(\frac{1.83}{6.5}\right) \\ &= 15.55 \text{ lb.}\end{aligned}$$

The load developed in the skirt reinforcement band can be calculated from the geometry of Figure 18 as follows:

$$\begin{aligned}P_{\text{dev}} &= P_{\text{sb}} \\ &= \left(\frac{P_{\text{H}}}{2}\right) \text{ctn } \alpha \\ &= \left(\frac{15.55}{2}\right)(5.671) \\ &= 44.0 \text{ lb.}\end{aligned}$$

The allowable load in the reinforcement tape which has a 350-lb ultimate tensile strength is

$$\begin{aligned}P_{\text{all}} &= \frac{350}{4.15} \\ &= 84.4 \text{ lb.}\end{aligned}$$

The margin of safety for the tape is

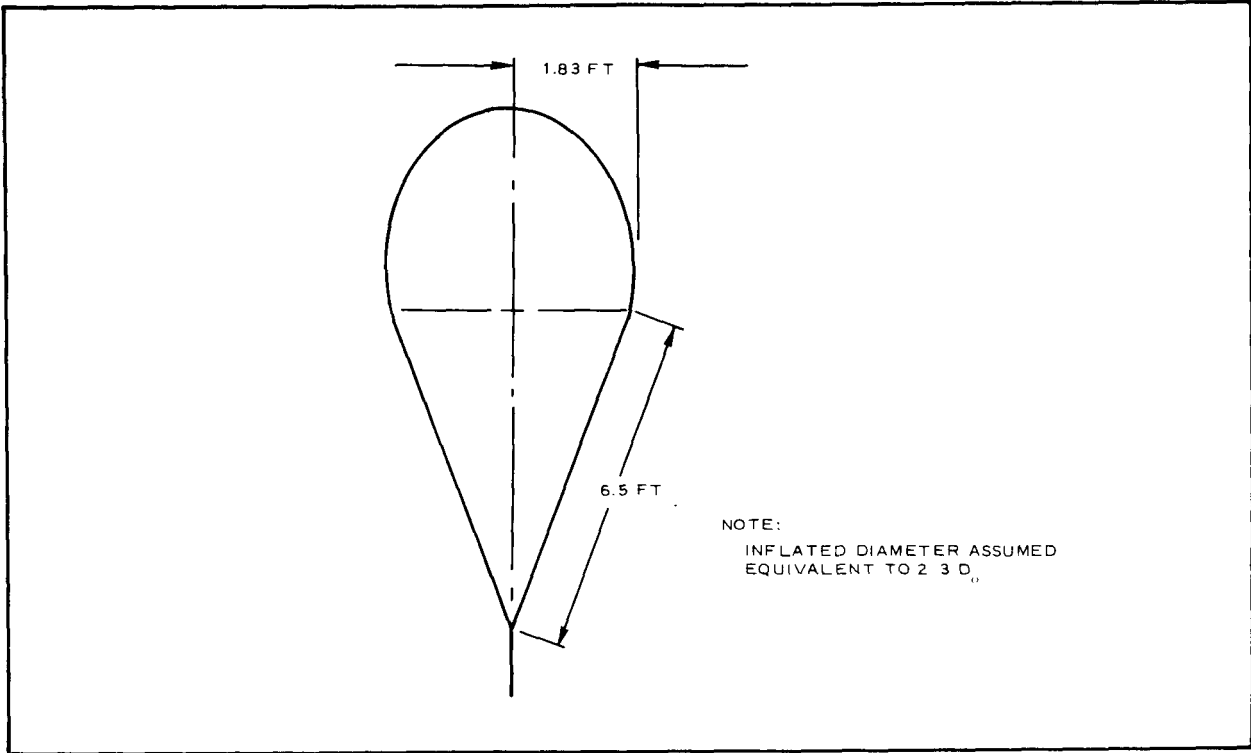


Figure 17 - Ringsail Inflated Geometry

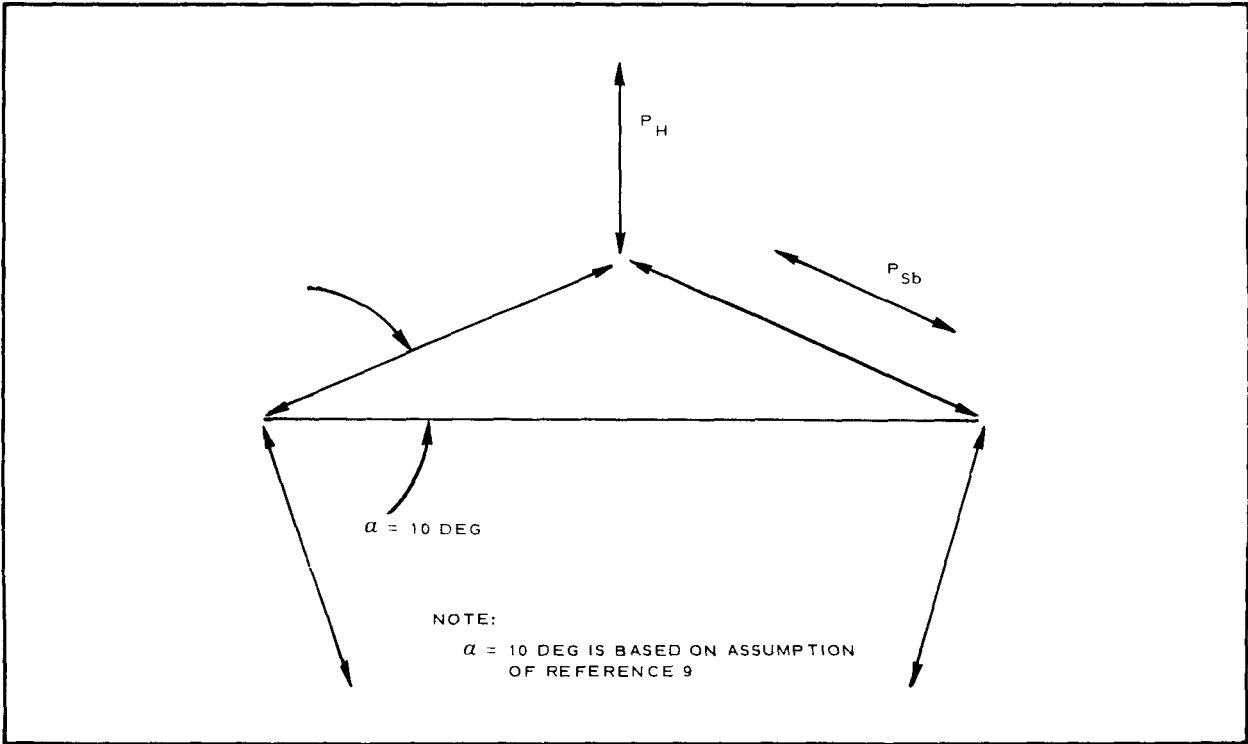


Figure 18 - Free Body Diagram of Skirt Reinforcement Band

$$\begin{aligned} \text{M.S.} &= \left(\frac{84.4}{44} \right) - 1.0 \\ &= 0.92 \end{aligned}$$

On the basis of Reference 9, the use of a vent tape seven percent shorter than the constructed vent diameter allows the vent tapes to carry at least 20 percent of P_H . The load developed in the vent reinforcement band can be calculated from the geometry of Figure 19 as follows:

$$\begin{aligned} P_{\text{dev}} &= P_{\text{vb}} \\ &= \frac{P_v}{2 \sin \alpha} \\ &= \frac{(12.46)}{2 \sin \left(\frac{360}{60} \right)} \\ &= 59.5 \text{ lb.} \end{aligned}$$

The allowable load for the reinforcement band which has a 350-lb ultimate tensile strength is

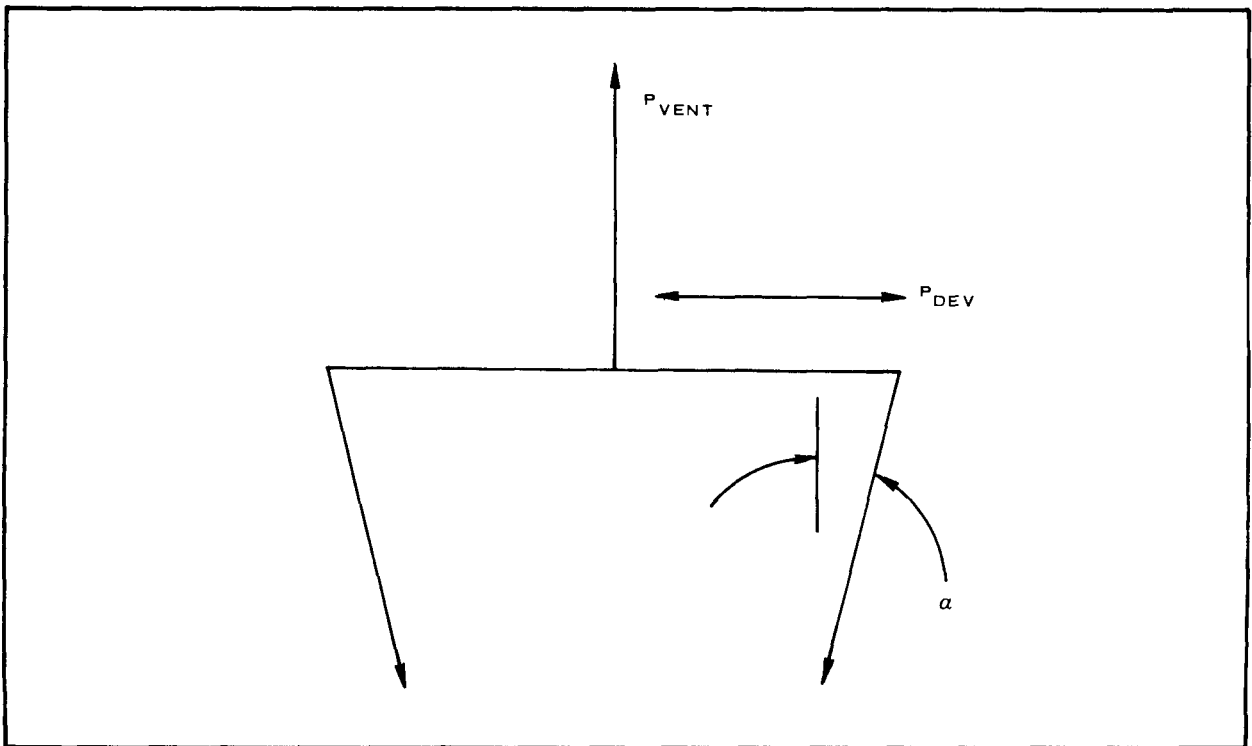


Figure 19 - Free-Body Diagram of Vent Reinforcement Band

$$P_{\text{all}} = \frac{350}{4.15}$$

$$= 84.3 .$$

The margin of safety of the band is

$$\text{M. S.} = \left(\frac{84.3}{59.5} \right) - 1.0$$

$$= 0.42 .$$

BALLUTE Inlet Design

General. - The use of an apex inlet in combination with small side inlets for final pressurization of a BALLUTE shows promise (References 10 and 11) in reducing the number and size of present side inlets. On the basis of results reported in Reference 10, an apex inlet for supersonic application must contain a check valve to preclude reverse flow and resultant partial inflation. While these BALLUTES used a hard apex inlet and check valve assembly, it is desirable that the inlet design be packageable, essentially independent of packing container constraints.

The purpose of the current investigation is to evaluate the effectiveness of a "soft" inlet and check valve in reducing BALLUTE filling times on a small-scale basis. To evaluate the apex inlet effectiveness, standard BALLUTE configurations (side inlets only) and modified configurations (apex and side inlets) were fabricated. The side inlets were the same design and size for both configurations. Filling time data from high-speed film coverage will provide the inflation times for each configuration to permit the relative effect of the apex inlet to be evaluated.

The basic gore pattern for the two configurations is the same as that used for a previous BALLUTE flight test (Reference 6); whereas, the side inlets are similar to those of the PRIME BALLUTE (Reference 12). A burble fence having a height equivalent to 10 percent of the BALLUTE envelope equatorial diameter was used. Because the purpose of the current investigation is aerodynamic rather than structural in nature, the stress analysis of the above referenced flight unit has been used as the basis of selecting the materials for the current configuration designs. This is a conservative approach because the deployment dynamic pressure was 250 psf for the flight unit compared to 120 psf for the wind-tunnel models.

Inlet Sizing. - The apex and side inlets were sized to be individually capable of inflating the BALLUTE in approximately one second for a free-stream Mach number of 3.0 and a free-stream dynamic pressure of 120 psf. The one-second inflation capability of each type of inlet should provide a sufficient difference in inflation time for the two configurations to permit evaluation of the effect of the apex inlet.

An analytical method, as described in Appendix A, previously developed and programmed for calculating the inflation time and internal pressure of BALLUTE decelerators was used to size the apex and side inlets (Reference 17). A wake predictive technique (References 13 and 14) was used to calculate the forebody wake properties that constitute the effective free stream of the BALLUTE.

These properties are presented in Figure 20 at an x/D of 3.0 aft of a 120-deg sharp-angle cone. The x/D value of 3.0 corresponds to the location of the BALLUTE confluence point. These wake properties were averaged and then used as inputs to the inflation analysis to determine the required inlet area to achieve the desired filling times. This analysis indicated that an apex inlet area of 7.2 sq in. and a total side inlet area of 16.8 sq in. are required. The side inlet area of 16.8 sq in. results in four 2.38-in. -diameter inlets.

Apex Inlet Design. - The basic inlet and valve design is presented in Figure 21. The valve assembly is retained within the BALLUTE envelope by means of a nylon tube assembly. This tube assembly in combination with the tensioning web serves as a positive means of erecting the inlet normal to the flow. The meridional tapes were extended at a more shallow apex angle than the 80-deg confluence angle to provide stronger inflation tendencies.

The meridional extension blockage of the inlet was accounted for as shown in Figure 22. The sum of the projected open areas equated to the required inlet

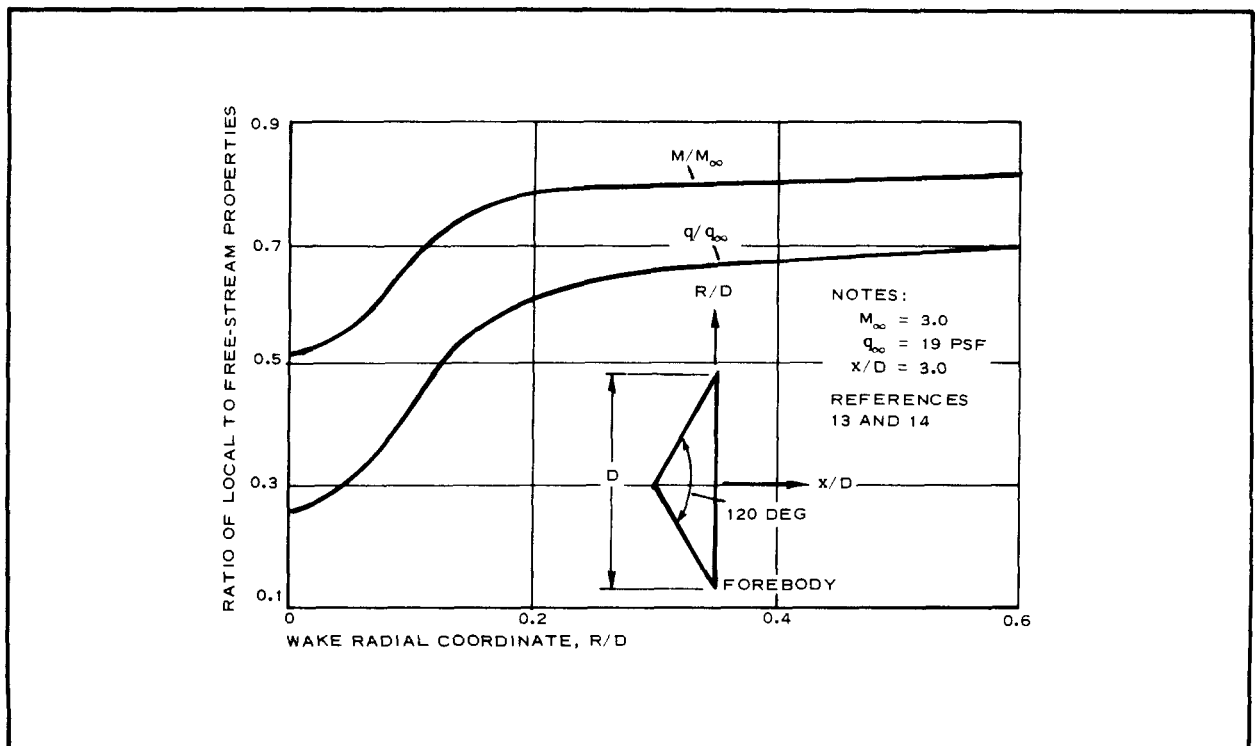


Figure 20 - Predicted Wake Properties Aft of 120-Deg Cone

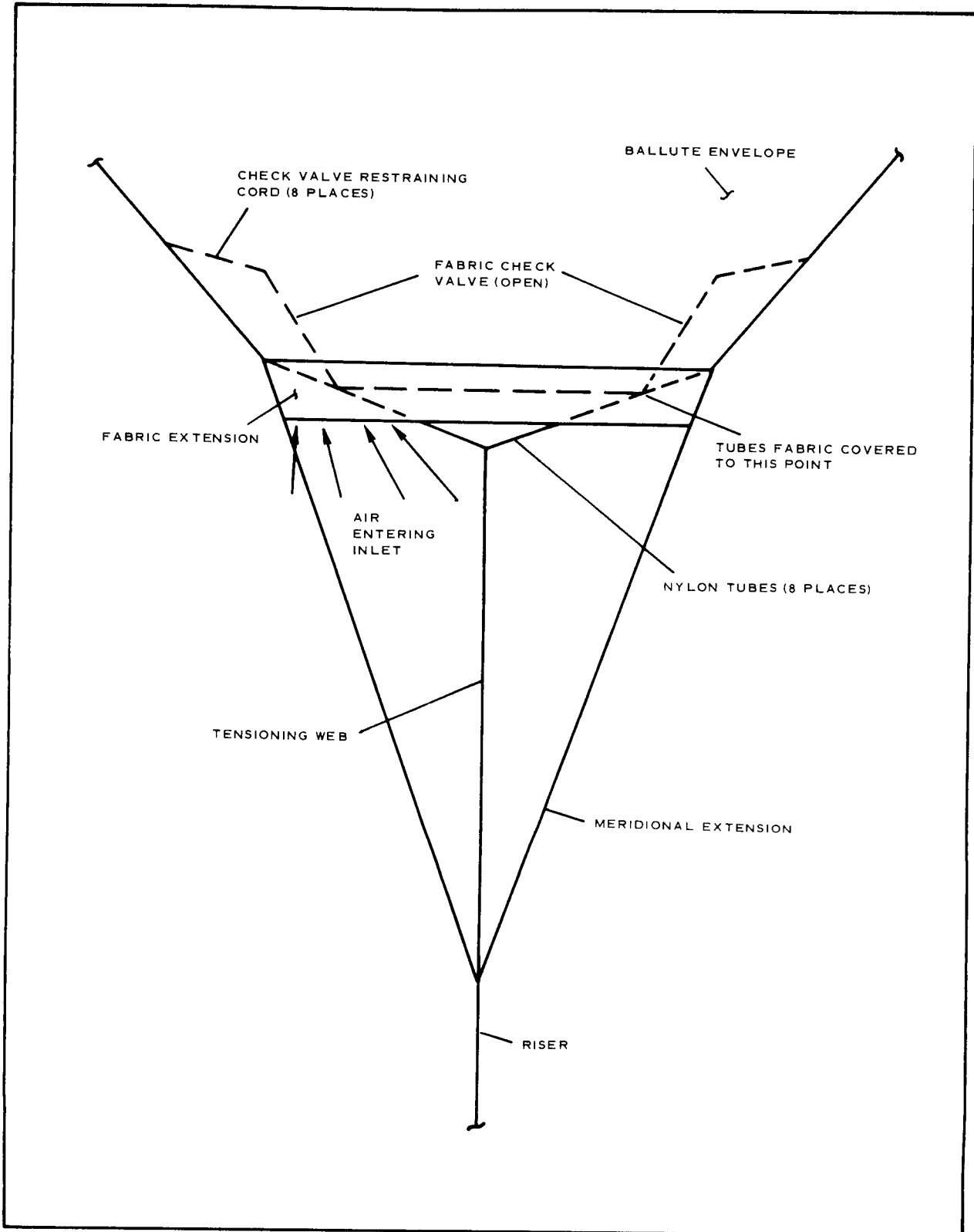


Figure 21 - Apex Inlet and Valve Design

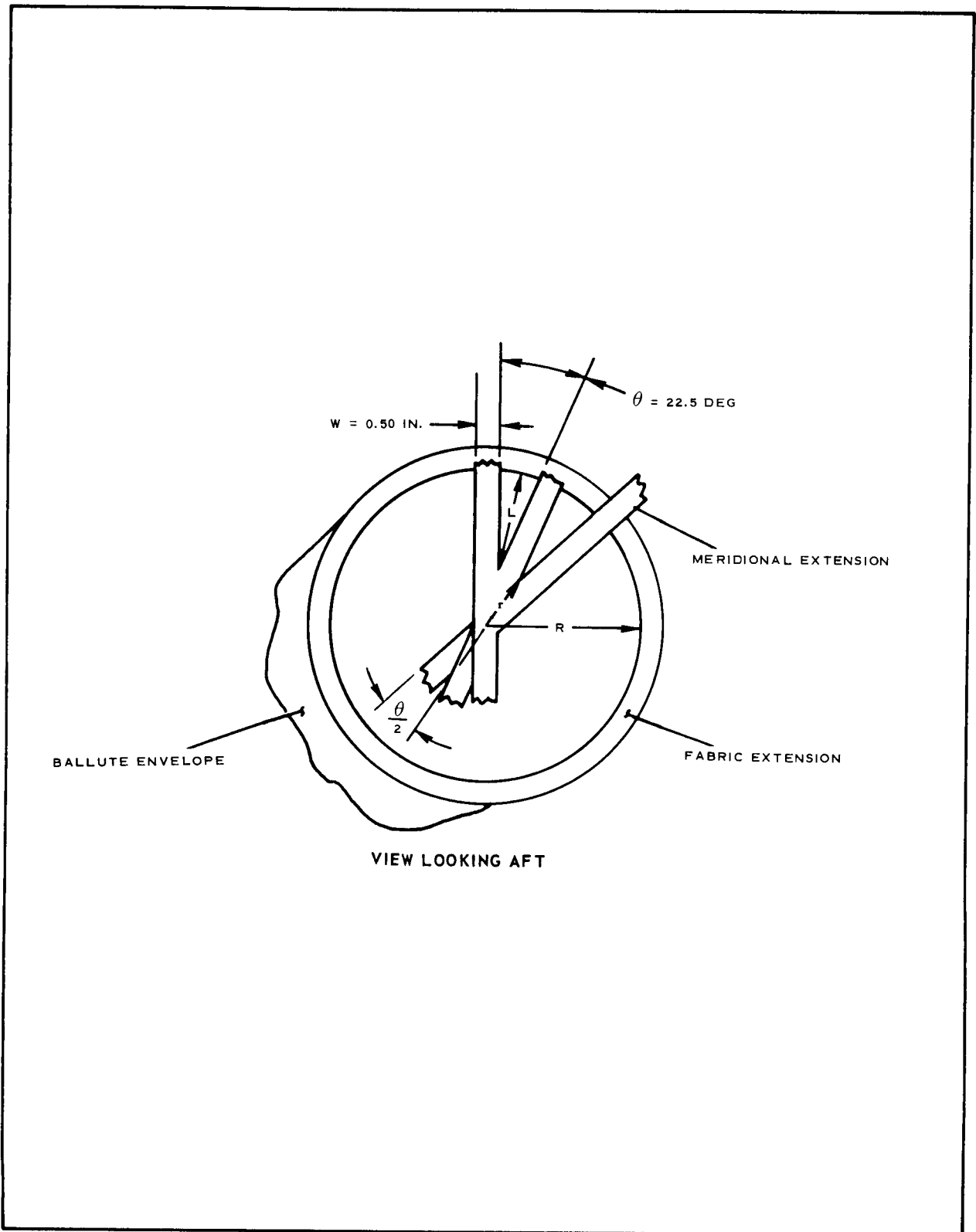


Figure 22 - Blockage of Inlet by Meridional Extensions

area (A) of 7.2 sq in. such that the required diameter of the BALLUTE opening then can be found as follows:

$$\frac{A}{16} = \frac{\pi L^2 \theta}{360}$$

Therefore,

$$L = \left[\frac{(7.2)(360)}{\pi \theta} \right]^{1/2}$$

$$= 1.52 \text{ in.}$$

From the geometry of Figure 22, $r = 0.25/\sin \theta/2 = 1.28 \text{ in.}$ and $R = L + r$; therefore,

$$R = 1.52 + 1.28$$

$$= 2.80 \text{ in.}$$

To establish the remaining inlet geometry, it was assumed the flow entering the BALLUTE turns through a maximum angle (α) as shown in Figure 23.

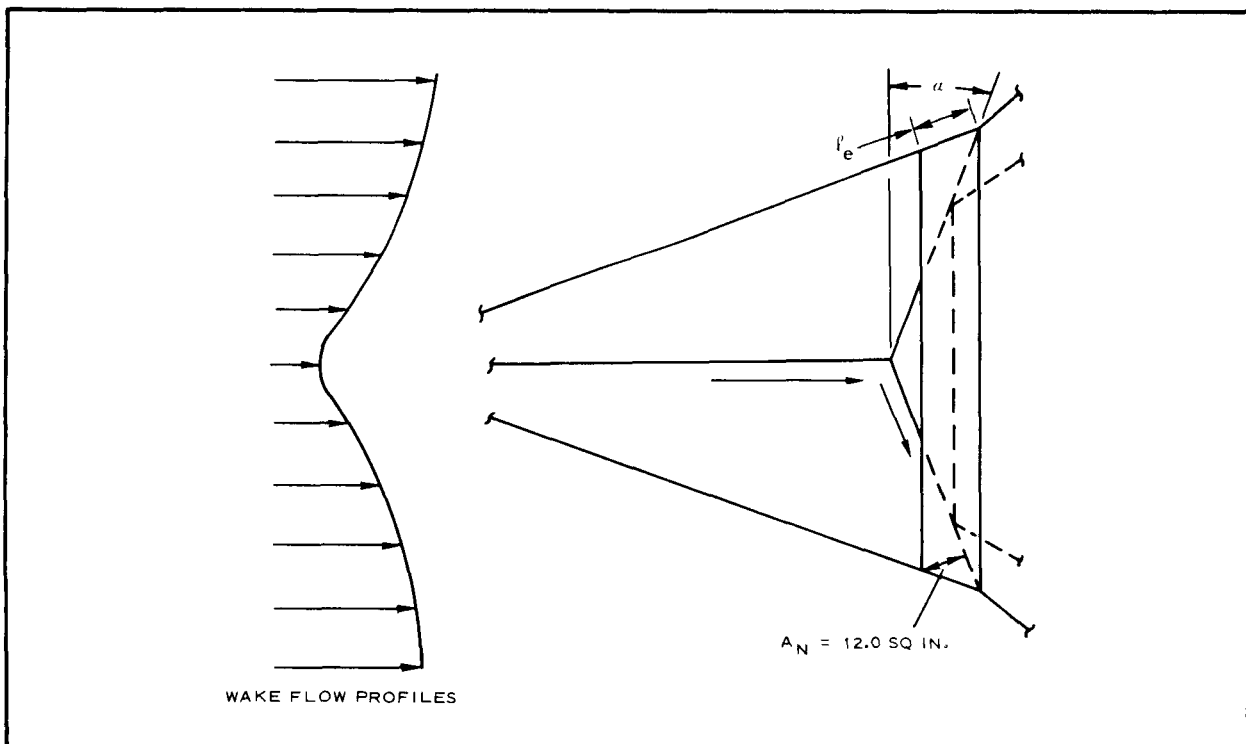


Figure 23 - Flow Entering Apex Inlet

The length (l_e) of the fabric extension shown in the figure then was selected such that the area (A_N) of 12.0 sq in., which is shown normal to the flow that has turned through an angle α , was greater than the required inlet area of 7.2 sq in. The flow turning through an angle less than α sees an area greater than that of A_N . To preclude restriction of the flow at the valve, the sum of the open area between the nylon tubes, when the valve is in the open position, is 16.0 sq in.

Static Inflation Tests. - For the inlet valve to be effective, *i. e.*, to preclude reverse flow through the apex inlet and permit the BALLUTE to fill completely, it must be capable of effectively sealing at a differential pressure equal to or smaller than that available in the wind tunnel. The differential pressure at which the inlet does seal was obtained by pressure measurements during static inflation tests. The minimum pressure measured with the apex inlet sealed and the side inlets tied off except for one through which the air supply was introduced was 25.0 psf.

An estimate of the differential pressure available under the wind tunnel test conditions is made in the following paragraphs and is compared to the required differential value of 25.0 psf.

The external pressure (P_e) acting on the valve is assumed equivalent to the wake total pressure (P_T) at a nondimensional radial coordinate (R/D) equal to the radius of the apex inlet as shown in Figure 24. The figure presents

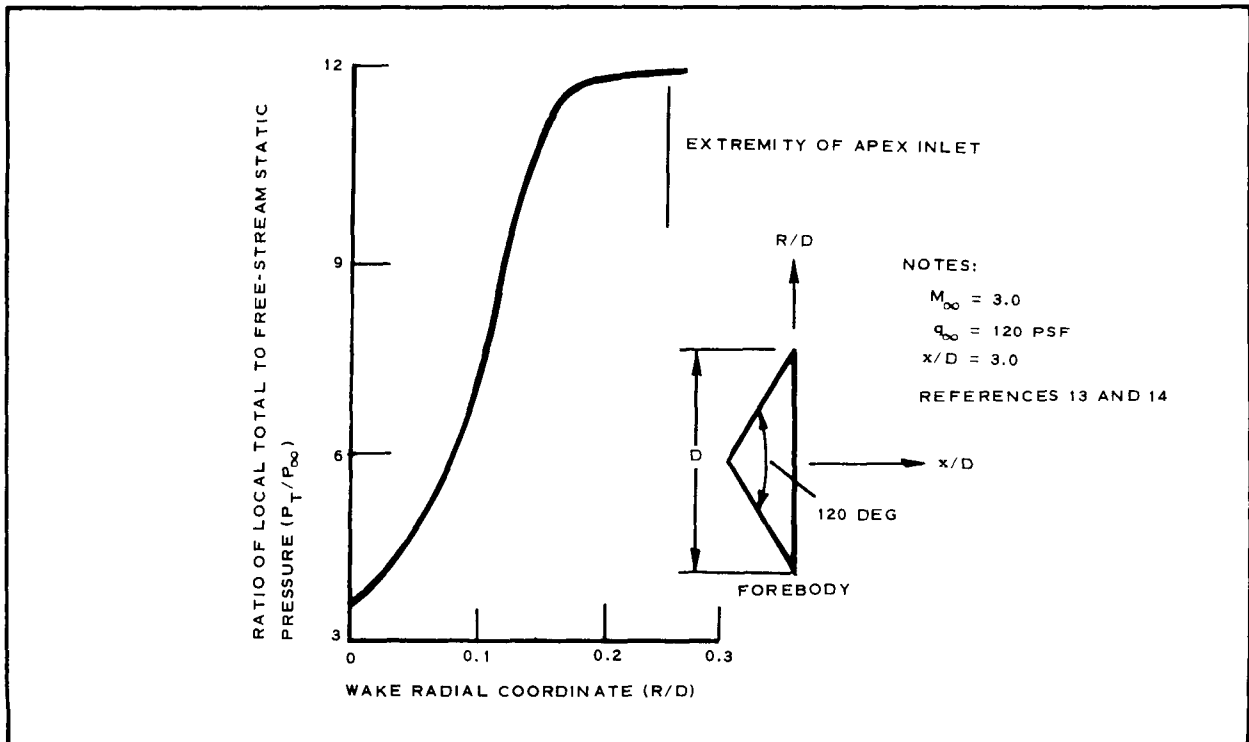


Figure 24 - Predicted Ratio of Wake Total Pressure to Free-Stream Static Pressure for 120-Deg Cone

the ratio of the wake total pressure (P_T) to free-stream static pressure (P_∞) versus the nondimensional radial coordinate (R/D) at an x/D of 3.0. The forebody is a 120-deg sharp-angle cone.

For a free-stream Mach number of 3.0 and a dynamic pressure of 120 psf, the free-stream static pressure is

$$\begin{aligned}P_\infty &= \frac{q_\infty}{0.7 M_\infty^2} \\&= \frac{120}{(0.7)(3)^2} \\&= 19 \text{ psf.}\end{aligned}$$

For the maximum P_T/P_∞ ratio of 12.0 from Figure 24 and the P_∞ value of 19.0 psf, the external pressure acting on the valve is

$$\begin{aligned}P_e &= P_T \\&= (12.0)(19.0) \\&= 228 \text{ psf.}\end{aligned}$$

The final internal pressure acting on the valve can be determined from the relation

$$C_{P_i} = \frac{(P_L - P_\infty)}{q_\infty}.$$

Actual BALLUTE internal pressure coefficients as a function of Mach number are presented in Figure 25.

For $M_\infty = 3.0$, the value for C_{P_i} is 2.3 and the resulting internal pressure is

$$\begin{aligned}P_i &= P_L \\&= (2.3)(q_\infty) + P_\infty \\&= 276 + 19 \\&= 295 \text{ psf.}\end{aligned}$$

The resulting differential pressure available to effect inlet closure is

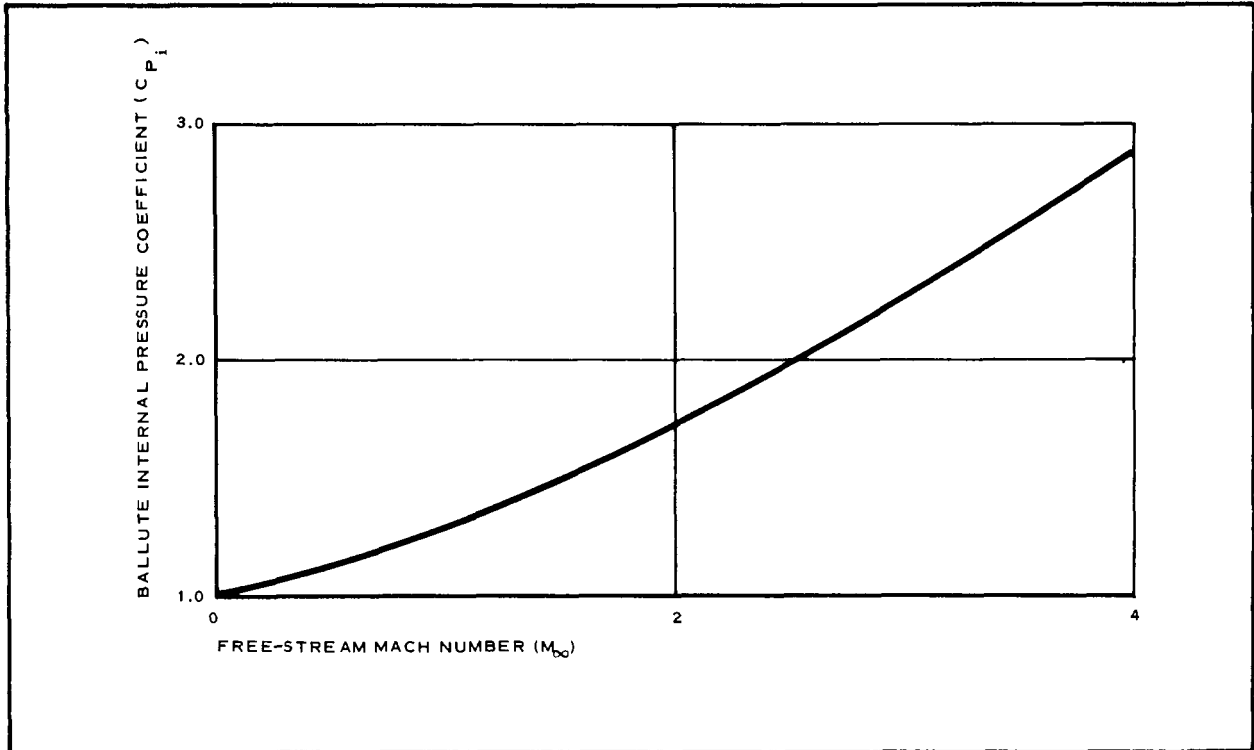


Figure 25 - BALLUTE Internal Pressure Coefficient versus Free Stream

$$\begin{aligned}
 \Delta P &= P_i - P_e \\
 &= 295 - 228 \\
 &= 67 \text{ psf.}
 \end{aligned}$$

Therefore, it can be concluded, on the basis of a required differential of 25 psf and an available differential conservatively estimated at 67 psf, that the valve assembly will close and permit full inflation of the BALLUTE.

During the static inflation tests, the leak rate of the modified BALLUTE was measured at several different internal pressures. The results of these and similar measurements for BALLUTES without apex inlets, which have inflated properly under actual application, are presented in Figure 26. It can be seen that the leak rate of the modified BALLUTE compares favorably with previous measurements for BALLUTE decelerators. It is reasonable then to assume that the leakage rate in the apex area of the modified configuration is not significantly different from the rate in the apex area of BALLUTES without the apex inlet. The above measurements provide additional assurance of the proper functioning of the valve and subsequent full inflation of the BALLUTE.

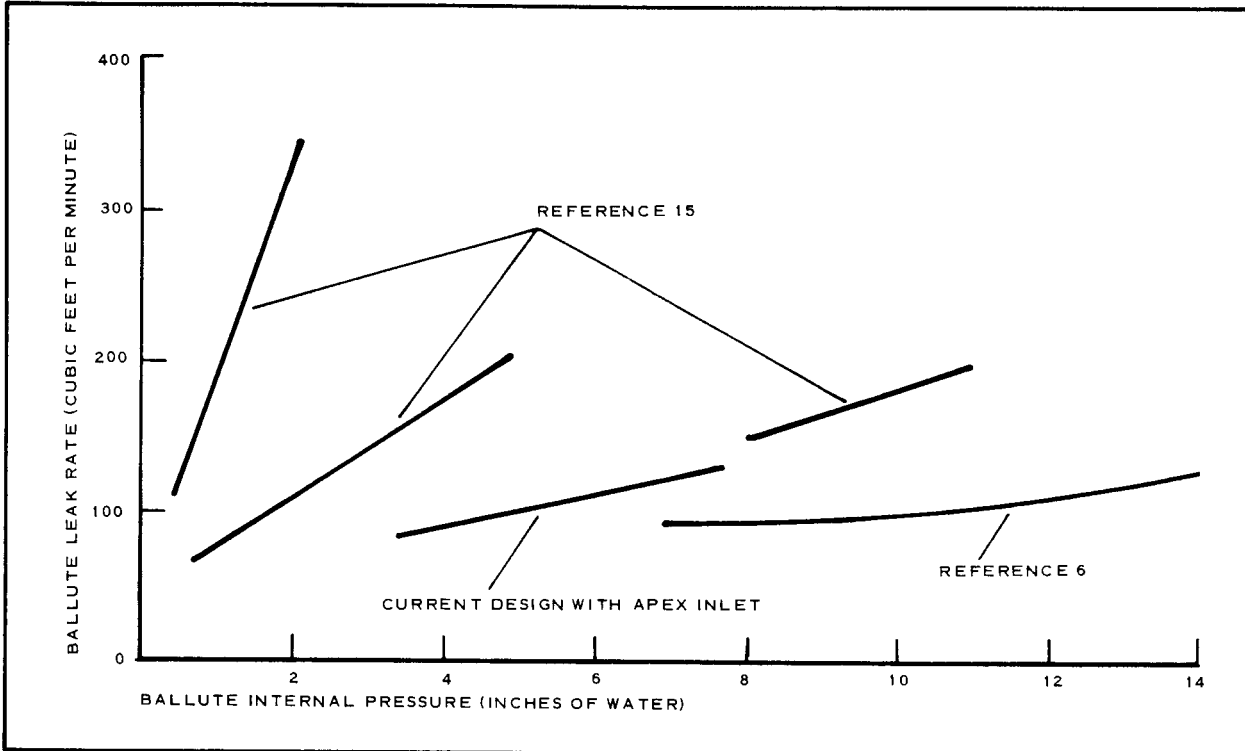


Figure 26 - BALLUTE Leak Rate versus Internal Pressure

Connector Link, Riser, Swivel, and Bridle

To facilitate decelerator model change and installation during testing, the use of a common riser, swivel, and bridle design was adopted.

The load developed in the connector link, riser, and swivel, dictated by the parachute design requirements of Section II, is

$$\begin{aligned}
 P_{\text{dev}} &= F_o \\
 &= C_{D_o} S_o q_{\infty} \\
 &= (1.0)(23.67)(70) \\
 &= 1663 \text{ lb.}
 \end{aligned}$$

The allowable load in the connector link, which has an ultimate tensile strength of 6000 lb, is

$$\begin{aligned}
 P_{\text{all}} &= \frac{6000}{2.0} \\
 &= 3000 \text{ lb,}
 \end{aligned}$$

where the design factor of 2.0 is the safety factor used on all metal parts (see Table VI).

TABLE VI - STRENGTH-LOSS AND SAFETY FACTORS
(ANCILLARY EQUIPMENT)

Symbol	Factor	Riser	Bridle	Connector link	Swivel
m	Joint efficiency	0.80	0.80	1.0	1.0
e	Abrasion	0.95	0.95	1.0	1.0
j	Safety	3.00	3.00	2.0	2.0
c	Line convergence	1.00	1.15
f	Asymmetrical loading	1.05	1.00	1.0	1.0
$\frac{jcf}{me}$	Design	4.15	4.55	2.0	2.0

The margin of safety in the connector link is

$$\begin{aligned} \text{M. S.} &= \left(\frac{6000}{3000} \right) - 1.0 \\ &= 1.0 . \end{aligned}$$

Using the appropriate design factor from Table VI, the allowable load in the riser which has an ultimate tensile strength of 8000 lb (two 4000-lb webs) is

$$\begin{aligned} P_{\text{all}} &= \frac{8000}{4.15} \\ &= 1930 \text{ lb} . \end{aligned}$$

The margin of safety in the riser is

$$\begin{aligned} \text{M. S.} &= \frac{1930}{1663} - 1.0 \\ &= 0.16 . \end{aligned}$$

The allowable load in the swivel, which has an ultimate tensile strength of approximately 4200 lb, is

$$\begin{aligned} P_{\text{all}} &= \frac{4200}{2.0} \\ &= 2100 \text{ lb} . \end{aligned}$$

The margin of safety is

$$\begin{aligned} \text{M. S.} &= \left(\frac{2100}{1663} \right) - 1.0 \\ &= 0.26. \end{aligned}$$

The load developed in the bridle legs, where it assumed one leg could sustain a load of $F_o/2$, is

$$\begin{aligned} P_{\text{dev}} &= \frac{F_o}{2} \\ &= 832 \text{ lb.} \end{aligned}$$

The allowable load in each bridle leg, which has an ultimate tensile strength of 4000 lb, is

$$\begin{aligned} P_{\text{all}} &= \frac{4000}{4.55} \\ &= 880 \text{ lb.} \end{aligned}$$

The margin of safety for the bridle is

$$\begin{aligned} \text{M. S.} &= \frac{880}{832} - 1.0 \\ &= 0.06. \end{aligned}$$

Decelerator Packing Scheme

Parachute. - Both parachute configurations used the same packing scheme and deployment bag design. The manner in which the parachute gores are folded along the longitudinal axis of the canopy is illustrated in Figure 27. Subsequently, the canopy is accordion folded as shown in Figure 28 to permit insertion into the deployment bag. After placement of the canopy in the bag, the retaining flap loops are arranged as shown in Figure 29. The suspension lines are looped through the locking loop to retain the canopy in the bag during deployment of the suspension lines. The suspension lines, after being passed through the locking loop, are looped through the stowage loops to preclude entanglement during deployment.

Static deployment tests have indicated that Nomex, because of its inherent lubricity, is an effective material for the deployment-bag locking loop. Additionally, the application of a silicone base lubricant to the Nomex locking loop was found effective in minimizing the force necessary to deploy the canopy. The static deployment tests indicated a force of approximately four pounds is necessary to effect deployment of the canopy.

BALLUTE. - The BALLUTE gores were folded along the longitudinal axis of the envelope as shown in Figure 30. Subsequently, the gores were accordion folded as shown in Figure 31 prior to placement into the deployment bag.

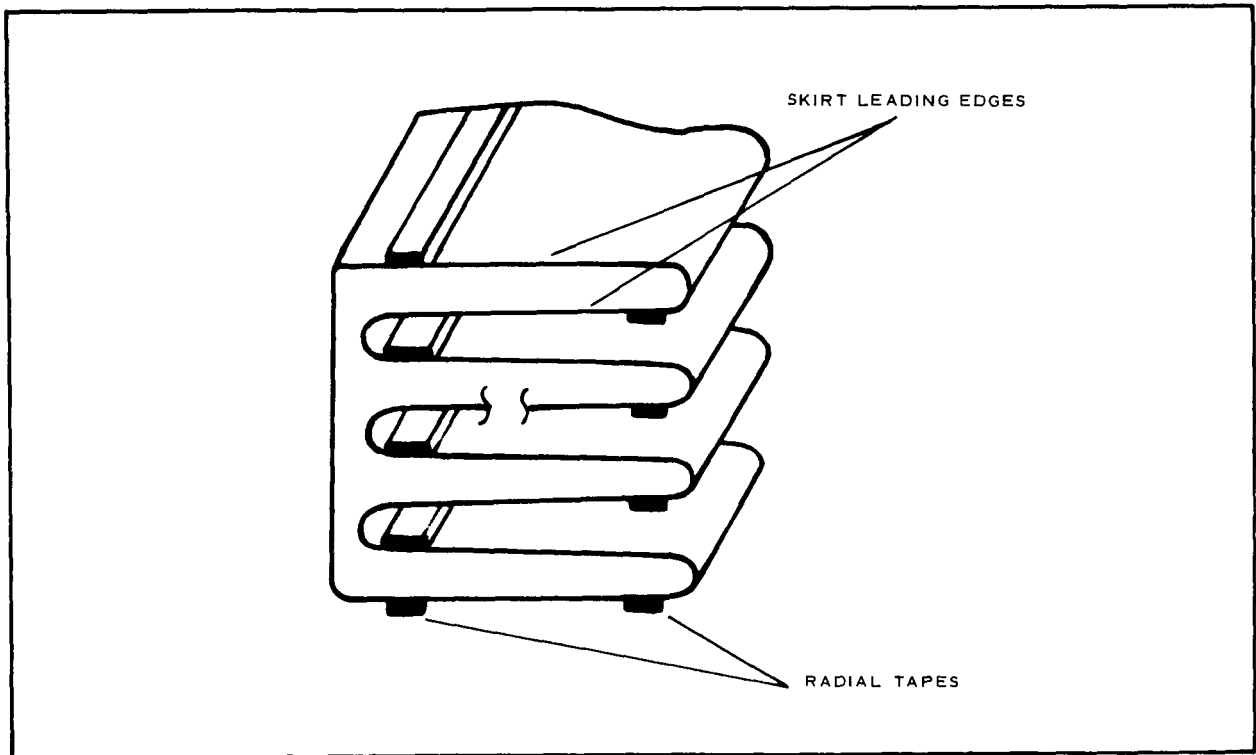


Figure 27 - Parachute Folded Longitudinally

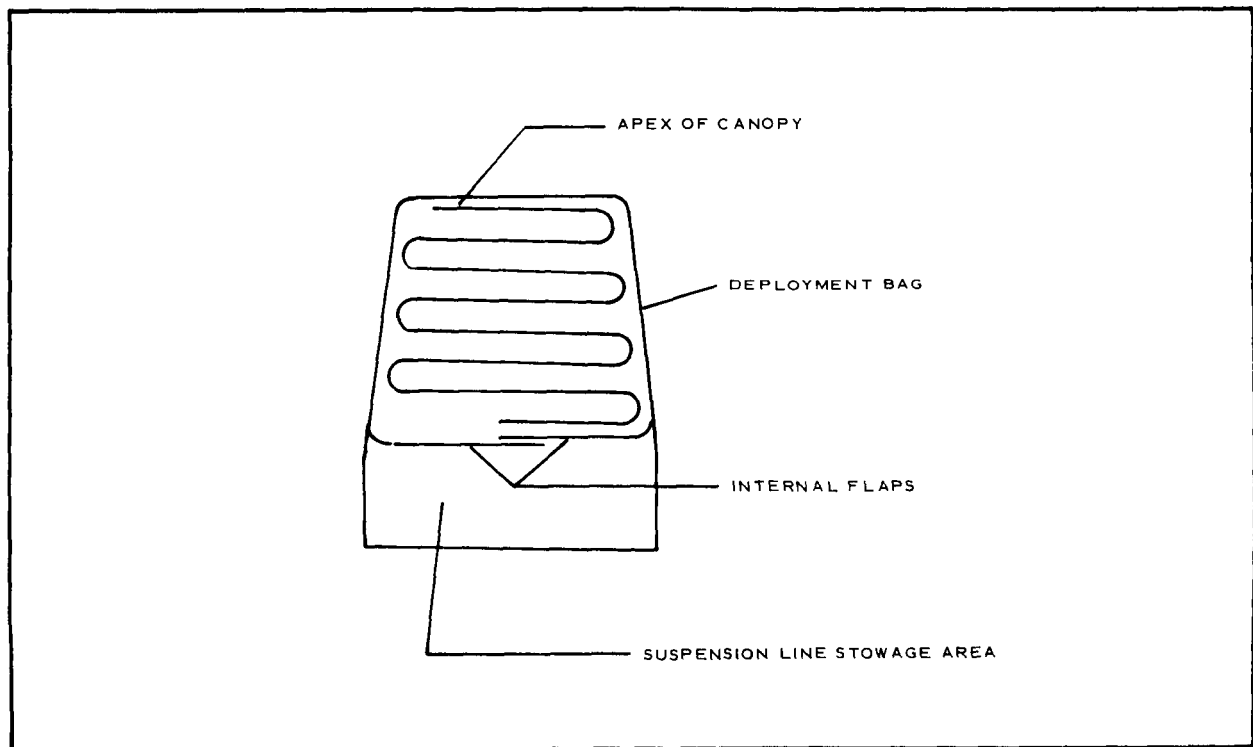


Figure 28 - Parachute in Deployment Bag

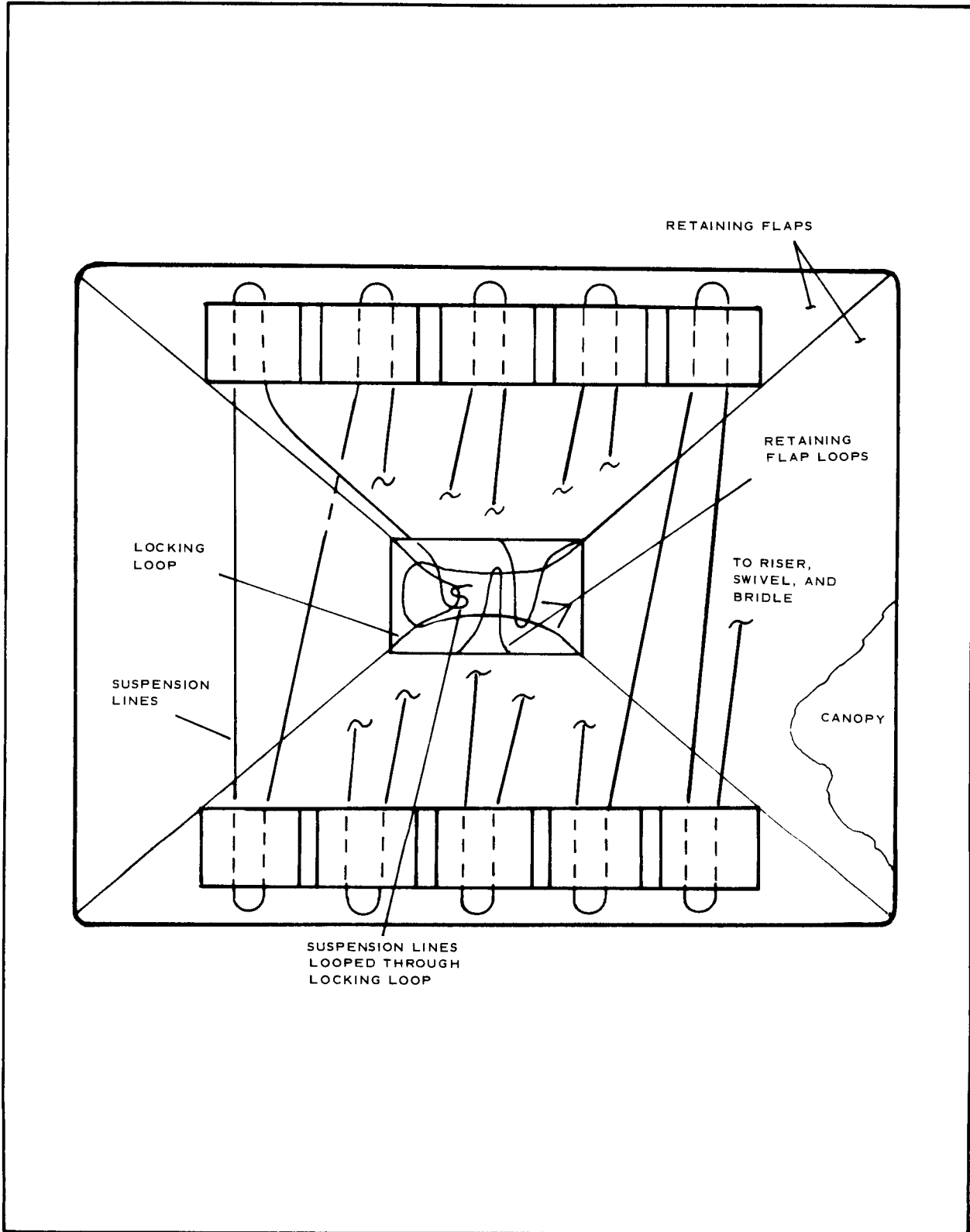


Figure 29 - Retaining Loop Arrangement

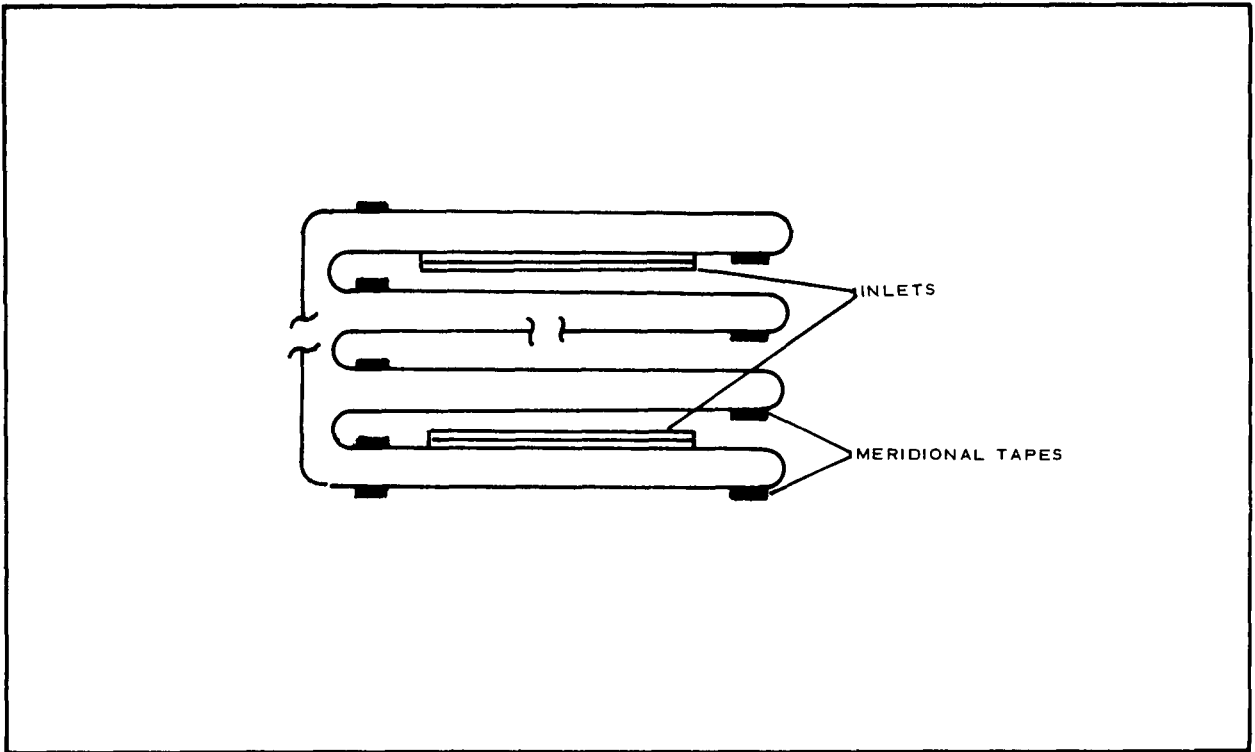


Figure 30 - BALLUTE Folded Longitudinally

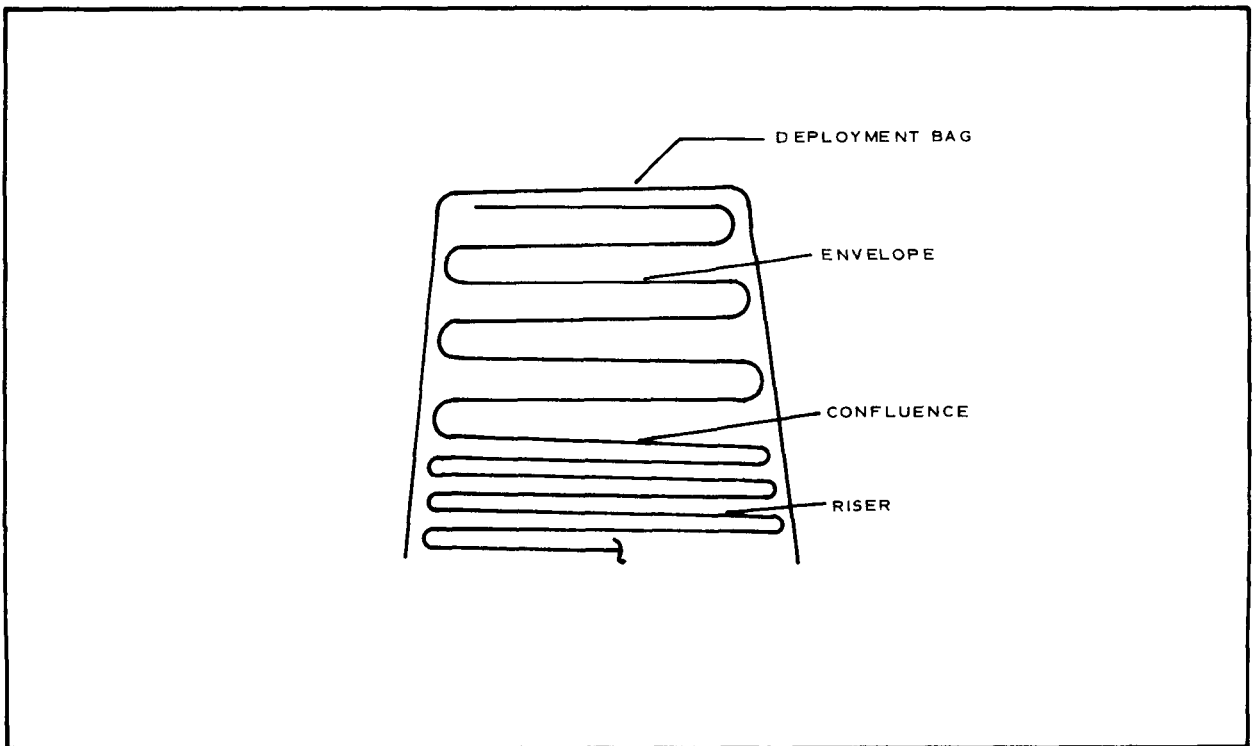


Figure 31 - BALLUTE in Deployment Bag

Material Selection for Fabric Decelerators

Dacron was used in the fabrication of all decelerator configurations while nylon was used in the riser and bridle. The suspension lines used were specially woven of dacron to the military specification listed in Table VI.

The permeability of the BALLUTE cloth was reduced to approximately 0.02 cfm/sq ft at a differential pressure of 0.5 in. of water by application of a neoprene elastomer. This lightweight coating does not restrict the cloth lobing capability nor does it lock in the yarns, which would result in lower seam efficiency. The cloth used for both the disk-gap-band and modified ringsail had a permeability of approximately 114 cfm^a/sq ft at a differential pressure of 0.5 in. of water.

A detailed summary of the materials for each decelerator configuration, selected to meet the structural requirements of Section II, are summarized in Table VII.

Pressure Model Design

General. - In the design of wind-tunnel pressure models, conservative methods of analysis and factors of safety are typically used since failure of a model can cause substantial damage to the tunnel installation. The subsequent model designs reflect methods of analysis and factors of safety similar to that required by Reference 20.

BALLUTE Design. - The inflated shape of the six-inch-diameter BALLUTE pressure model is the same as the shape of the standard fabric configuration defined previously. The basic pressure model envelope consists of front and rear surfaces, spun from 0.04-in. AISI 305 stainless steel butted together over a coupling ring (see Figure 32). The burble fence and apex of the BALLUTE are machined from solid stainless. The four side inlets are constructed from low-carbon stainless tubing bent to the inlet shape. A detailed description of the materials and joining techniques used in the model design are provided in Figure 47. Attachment of the pressure model to the sting is accomplished by a three-member yoke (see Figure 32).

Pressure ports have been located in the front surface, burble fence, rear surface and each of the four side inlets of the BALLUTE. The pressure tubes exit the model through a circular opening in the center of the rear surface which is then slivered soldered closed. This approach will provide a minimum of interference with rear surface pressure measurements while maintaining simplicity in the design.

BALLUTE Stress Analysis. - The pressure model design is capable of withstanding loads imposed by a dynamic pressure during tunnel start-up of 500 psf. Additionally, the design analysis has accounted for normal forces sustained during angle-of-attack measurements. The maximum drag force the model is designed to sustain, considering a drag coefficient of 1.84 for a flat plate in supersonic flow (Reference 18), is

^aCubic feet per minute.

TABLE VII - DECELERATOR MATERIALS SUMMARY

Item	Component	Description	Tensile strength*
DGB and ring-sail parachute	Cloth	2.25 oz/sq yd dacron (Stern and Stern pattern 15004), nominal permeability [†] = 114 cfm/sq ft	80 lb/in.
	Radial and reinforcement tapes	0.50-in. -wide dacron (Bally Ribbon pattern 8290)	350 lb
	Suspension lines	Dacron, woven similar to MIL-C-7515, Type XI	300 lb
Parachute deployment bag	Riser	Nylon, MIL-W-5625	
	Cloth and retaining flaps	2.25 oz/sq yd dacron (Stern and Stern pattern 15004)	80 lb/in.
	Locking loop	Nomex, MIL-W-5625	1000 lb
BALLUTE	Cloth	4.35 oz/sq yd dacron (Stern and Stern pattern 15035), nominal permeability (after coating)* = 0.02 cfm/sq ft	200 lb/in.
	Meridional tapes	0.05-in. -wide dacron (Bally Ribbon pattern 8290)	330 lb
	Riser	Nylon, MIL-W-27657, Type II	4000 lb
BALLUTE deployment bag	Cloth	4.35 oz/sq yd dacron (Stern and Stern pattern 15035)	200 lb/in.
Swivel	. . .	Gould Laboratories part GL1844A-1	4200 lb
Connector link	. . .	Part MS22002-1	6000 lb

* Rated strength.

[†] Measured at 0.5-in. differential water pressure.

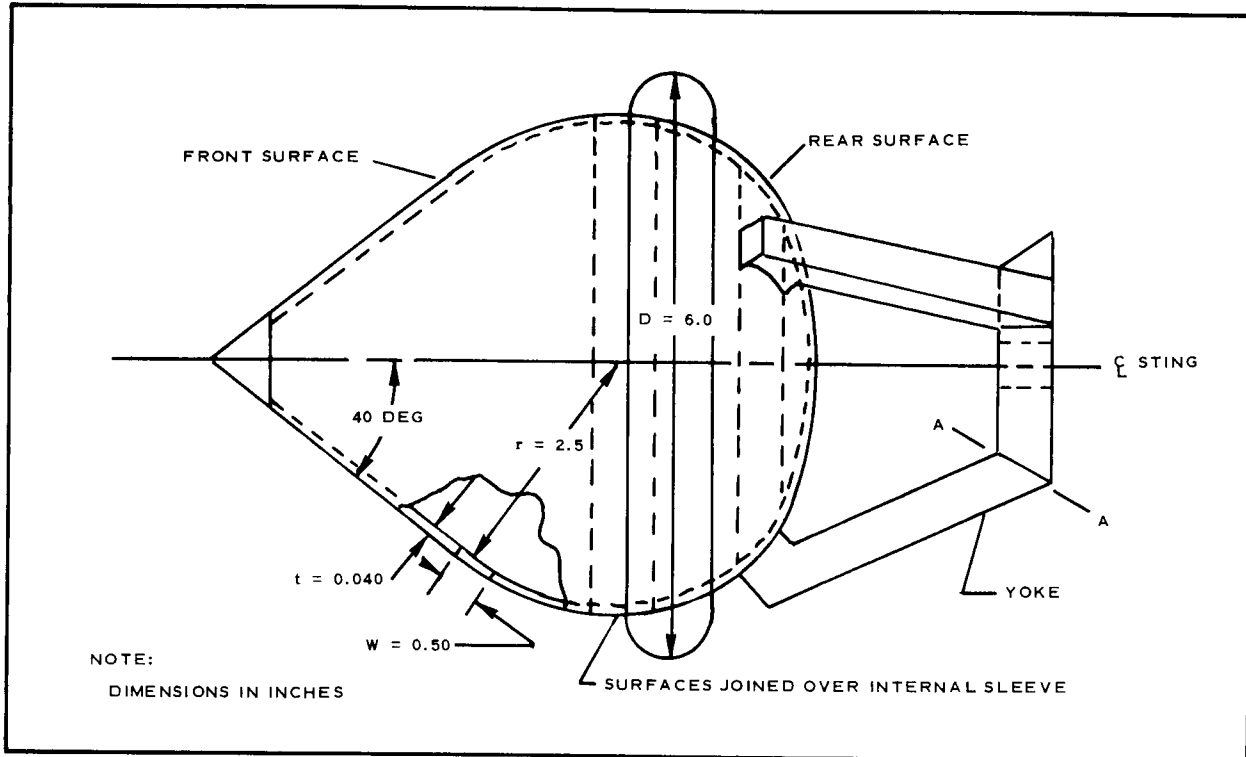


Figure 32 - BALLUTE Pressure Model

$$\begin{aligned}
 F_D &= C_D A q \\
 &= (C_D) \left(\frac{\pi D^2}{4} \right) (q) \\
 &= (1.84)(0.785) \left(\frac{6}{12} \right)^2 (500) \\
 &= 180 \text{ lb.}
 \end{aligned}$$

It is assumed that the maximum normal force will never exceed $0.75 F_D$

$$\begin{aligned}
 F_N &= 0.75 F_D \\
 &= 135 \text{ lb.}
 \end{aligned}$$

The maximum compressive stress in the BALLUTE skin can be determined, considering a pressure differential of 500 psf (acting on the 0.5-in. -wide ring section at the maximum radius of the front surface as shown in Figure 32), as follows

$$\begin{aligned}
 f_c &= \frac{pr}{t} \\
 &= \frac{\frac{500}{144} (2.5)}{0.04} \\
 &= 216 \text{ psi}
 \end{aligned}$$

which is well below the 35,000 psi allowable. The allowable pressure differential in the 0.5-in. ring section can be calculated from the relation

$$P_{\text{all}} = \frac{3EI}{r^3},$$

where

$$E = 29 \times 10^6 \text{ psi,}$$

and

$$\begin{aligned}
 I &= \frac{Wh^3}{12} \\
 &= \frac{(0.5)(0.04)^3}{12} \\
 &= 2.66 \times 10^{-6} \text{ in.}^4
 \end{aligned}$$

Therefore,

$$\begin{aligned}
 P_{\text{all}} &= \frac{(3)(29 \times 10^6)(2.66 \times 10^{-6})}{2.5^3} \\
 &= 14.84 \text{ psi.}
 \end{aligned}$$

Considering the available differential of 500 psf, the resulting factor of safety is

$$\begin{aligned}
 \text{F.S.} &= \frac{14.84}{\frac{500}{144}} \\
 &= 4.27.
 \end{aligned}$$

While axial and normal forces act simultaneously when the model is at an angle of attack, the maximum stress in the weld of A-A (see Figure 33) is obtained when considering only the maximum normal force.

Therefore, considering only the maximum normal force, the maximum compressive stress can be determined from the relation

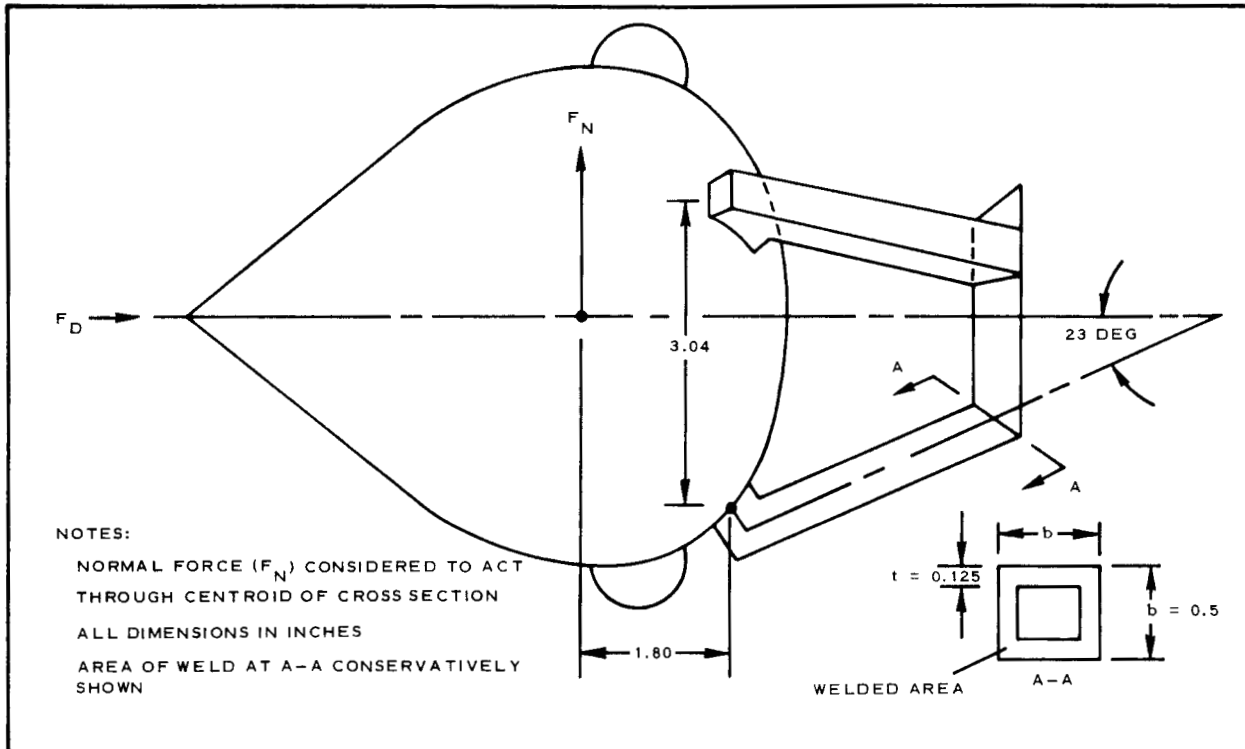


Figure 33 - Normal Force Acting on BALLUTE

$$f_c = \frac{P}{A} + \frac{Mc}{I},$$

From Figure 33 and the free-body diagram of Figure 34, the following are determined

$$P_N = \left(\frac{1.8}{3.04} \right) F_N$$

$$= \left(\frac{1.8}{3.04} \right) (135),$$

$$I = \left(\frac{bh^3}{12} \right) - \left(\frac{b'h'^3}{12} \right)$$

$$= \left[(0.05)(0.5)^3 \right] - \frac{(0.25)(0.25)^3}{12}$$

$$= 0.0048 \text{ in.}^4,$$

$$A = 2bt + 2t(b - 2t)$$

$$= 0.188 \text{ sq in.},$$

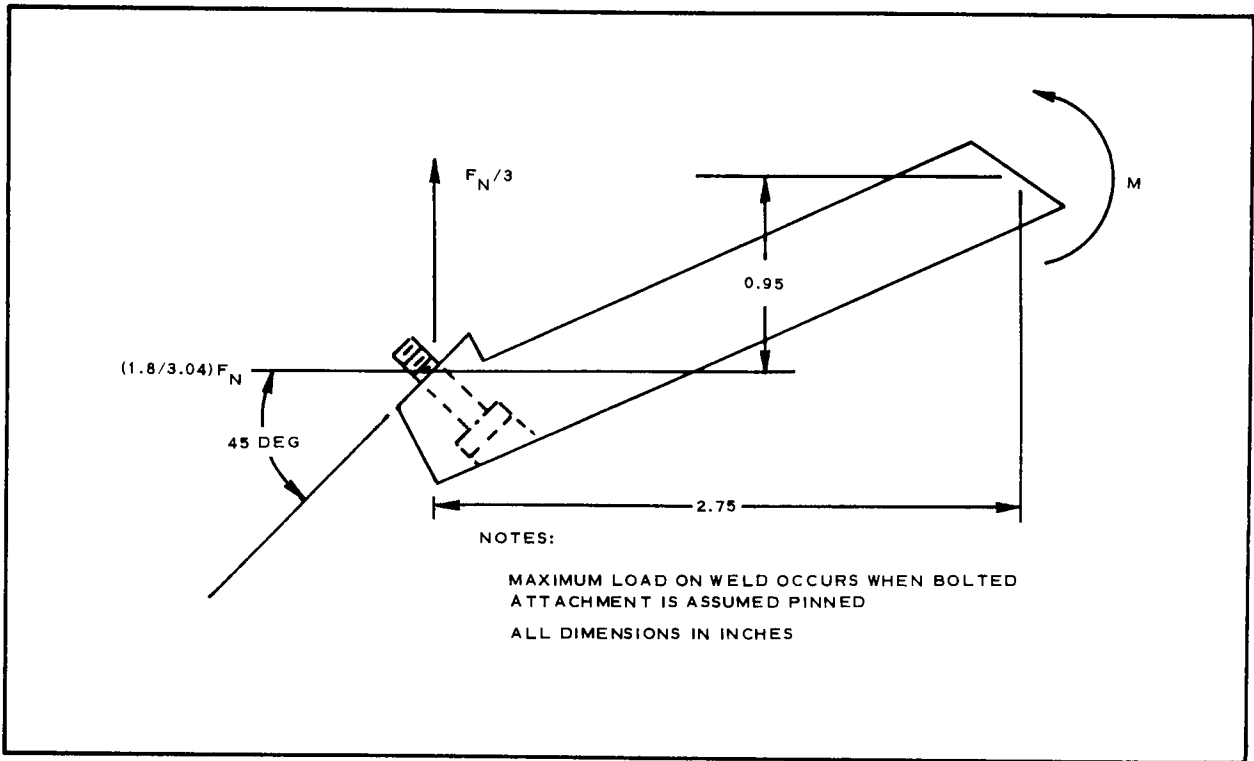


Figure 34 - Free-Body Diagram of Yoke Member

$$\begin{aligned}
 M &= 0.95P + 2.75 \frac{F_N}{3} \\
 &= (0.95)(80) + (2.75)(4.5) \\
 &= 200 \text{ in. -lb .}
 \end{aligned}$$

Therefore, the maximum compressive stress in the weld is

$$\begin{aligned}
 f_c &= \frac{80}{0.1875} + \frac{(200)(0.25)}{(0.00488)} \\
 &= 10,547 \text{ psi.}
 \end{aligned}$$

The factor of safety, considering an 80,000 psi allowable, is

$$\begin{aligned}
 \text{F.S.} &= \frac{80,000}{10,547} \\
 &= 7.6 .
 \end{aligned}$$

From the free-body diagram of Figure 35, considering the normal force only, the tension and shear load in the attachment screw are

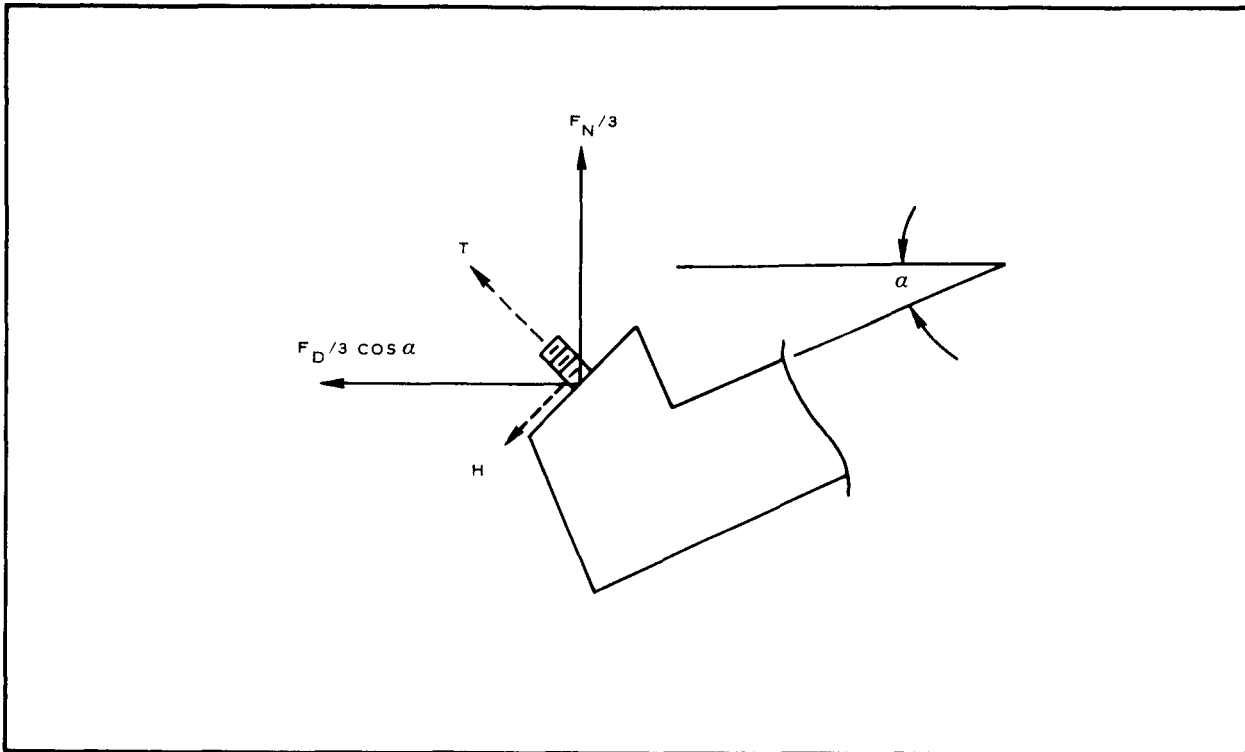


Figure 35 - Free Body of Model Attachment Screw

$$\begin{aligned} \text{Tension (T)} &= 0.707(80 + 45) \\ &= 88 \text{ lb,} \end{aligned}$$

and

$$\begin{aligned} \text{Shear (H)} &= 0.707(80 - 45) \\ &= 24.7 \text{ lb.} \end{aligned}$$

However, when considering the maximum drag force, the shear load in the screw at a 0-deg angle of attack is

$$\begin{aligned} H &= \frac{C_D A q}{3 \cos \alpha} \\ &= \frac{180}{3 \cos 23 \text{ deg}} \\ &= 65.2 \text{ lb.} \end{aligned}$$

Considering an allowable tensile load of 1120 lb and shear load of 670 lb, the minimum factor of safety is

$$\frac{670}{65.2} = 10.25 .$$

Parachute Design. - The inflated shape for the six-inch-diameter, 12.5-percent geometric porosity DGB was obtained from film data taken during the test of configuration 7 of Reference 5. The shape was recorded at a point where the parachute appeared to be in its most representative and stable condition ($M = 2.0$).

The 32 gore lobes of the parachute of configuration 7 were not included in the disk portion of the canopy design since measurement of their effect on the canopy pressures would be difficult in view of the size and number of gores of the model. In addition, it would be expected that this effect would be negligible. The parachute model consists of a front and rear section joined aft of the leading edge of the disk by a weldment as shown in Figure 36. The rear section of the canopy, spun from 0.063-in. AISI 305 stainless, has a 0.55-in. diameter vent at its center. The front section of the canopy is fabricated from 0.63-in. AISI 306 stainless flat stock. Each segment of the gap is milled from the flat stock as illustrated in Figure 37. Subsequently, the lobes are placed in the band portion of the canopy by hand forming each lobe around a 0.407-in.-diameter mandrel. Slight breaks in the flat stock, as shown in the figure, will facilitate the lobe forming operation. After forming the lobes, the band assembly is welded along its longitudinal axis. The completed band assembly is then attached to the rear section of the canopy as previously discussed.

Attachment of the model to the sting is accomplished by a three-member yoke similar to that used for the BALLUTE pressure model. Additional details relating to the materials and joining techniques used in the model design are presented in Section IV.

Two pressure model designs presented in Section IV permit measurement of internal and external pressures. The tubes for measuring the internal pressures pass over the exterior of the model and along the three members of the attachment yoke. The tubes for measuring the external pressures pass along the internal portion of the canopy and exit at the rear surface through one of three openings in the canopy. The openings then are sliver soldered closed after the tubes are passed through the canopy. The tubes then travel along one of the three members of the attachment yoke. The tubes passing through the canopy rear surface are sufficiently displaced from the canopy vent to preclude interference with flow through the vent.

Parachute Stress Analysis. - The parachute model was designed to withstand the same drag force as the BALLUTE model. It is assumed the maximum normal force will never exceed $0.50 F_D$.

Therefore,

$$\begin{aligned} F_N &= 0.5 F_D \\ &= (0.5)(180) \\ &= 90 \text{ lb.} \end{aligned}$$

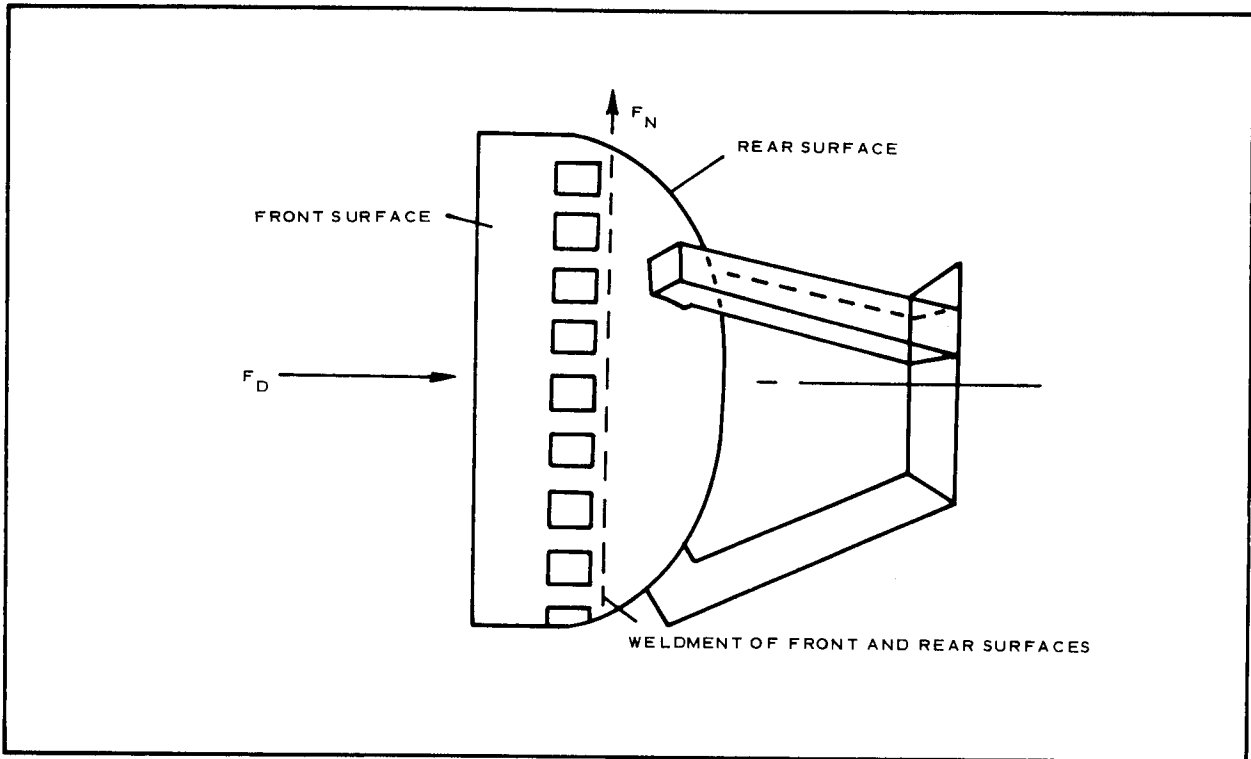


Figure 36 - DGB Pressure Model

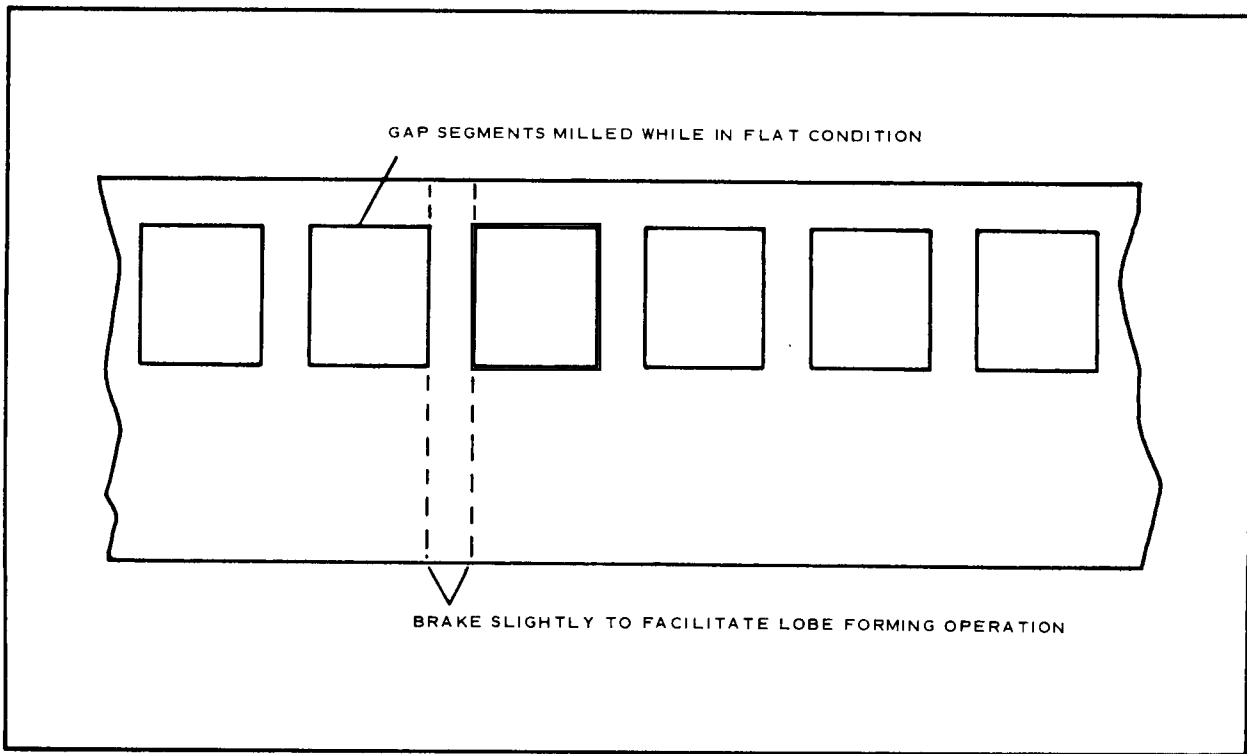


Figure 37 - Front Section of Canopy in Flat Condition

From the geometry of Figure 38, the possibility of buckling occurring at the local load (P) is determined as follows: the maximum bending stress at the local load is

$$\delta = \frac{CP}{2t},$$

where a value of C = 0.250 is taken from Reference 19 and

$$\begin{aligned} P &= \frac{C_D A_q}{3 \cos \alpha} \\ &= \frac{180}{3 \cos 28.5 \text{ deg}} \\ &= 68.3 \text{ lb.} \end{aligned}$$

Therefore,

$$\begin{aligned} \delta &= \frac{(0.25)(68.3)}{(0.063)^2} \\ &= 4300 \text{ psi.} \end{aligned}$$

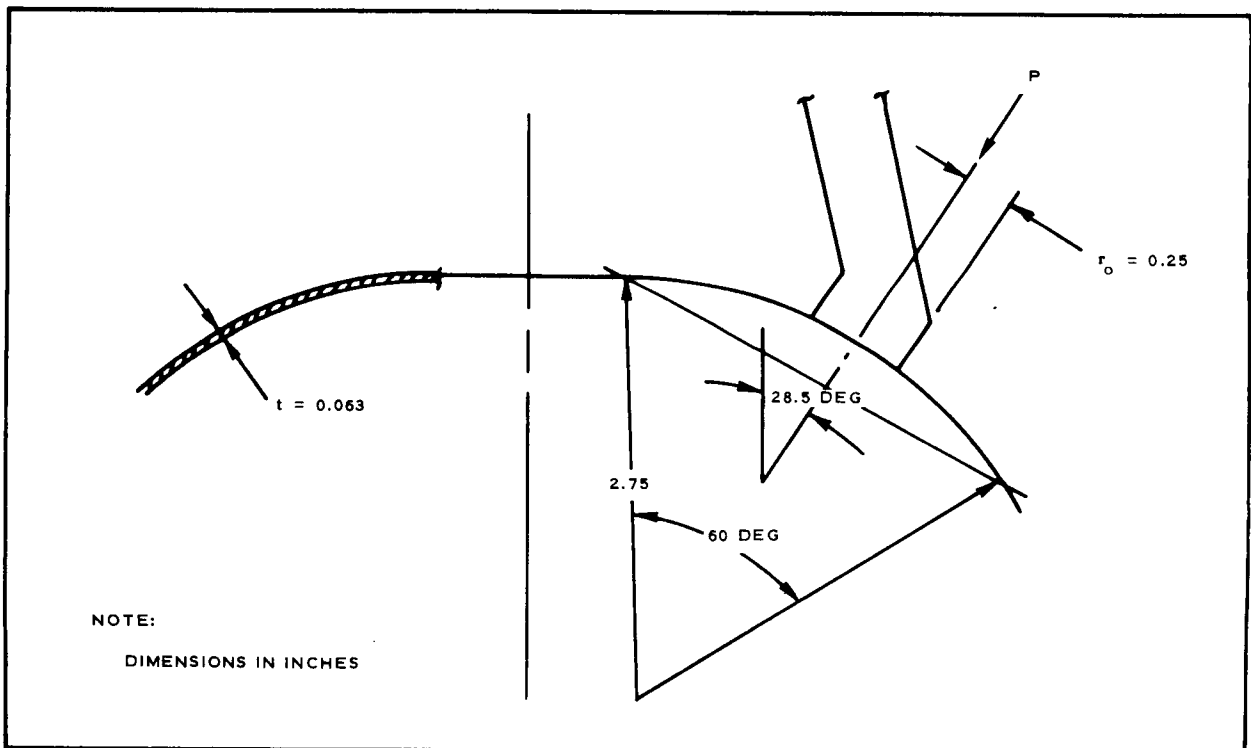


Figure 38 - Cross Section of Pressure Model

The maximum membrane stress at the local load is

$$\delta' = \frac{\beta P}{t},$$

where a value of $\beta = 0.137$ is taken from Reference 19. Therefore,

$$\begin{aligned}\delta' &= \frac{(0.137)(68.3)}{(0.063)^2} \\ &= 2350 \text{ psi.}\end{aligned}$$

The combined stress at the local load is

$$\begin{aligned}\delta_{\text{comb}} &= \delta + \delta' \\ &= 4300 + 2350 \\ &= 8650 \text{ psi.}\end{aligned}$$

The factor of safety, considering an allowable of 35,000 psi, is

$$\begin{aligned}\text{F.S.} &= \frac{35,000}{8,560} \\ &= 4.1.\end{aligned}$$

The stress developed in the elements connecting the band and disk can be determined, considering the distribution of the normal force shown in Figure 39, in the following manner.

Referring to Figure 40, the portion of the normal force carried by each element is proportional to its stiffness, with elements 9 and 25 carrying the maximum load. To determine this load, it was necessary to establish the moments of inertia of each of the 32 connecting elements about their neutral axis.

From the geometry of Figure 41, the approximate moment of inertia for an element is

$$\begin{aligned}I_{\text{NA}} &= \frac{bh^3}{12} \\ &\approx \frac{\left(\frac{t}{\cos \alpha}\right) (\cos \alpha)^3}{12},\end{aligned}$$

where for large values of α the relation becomes

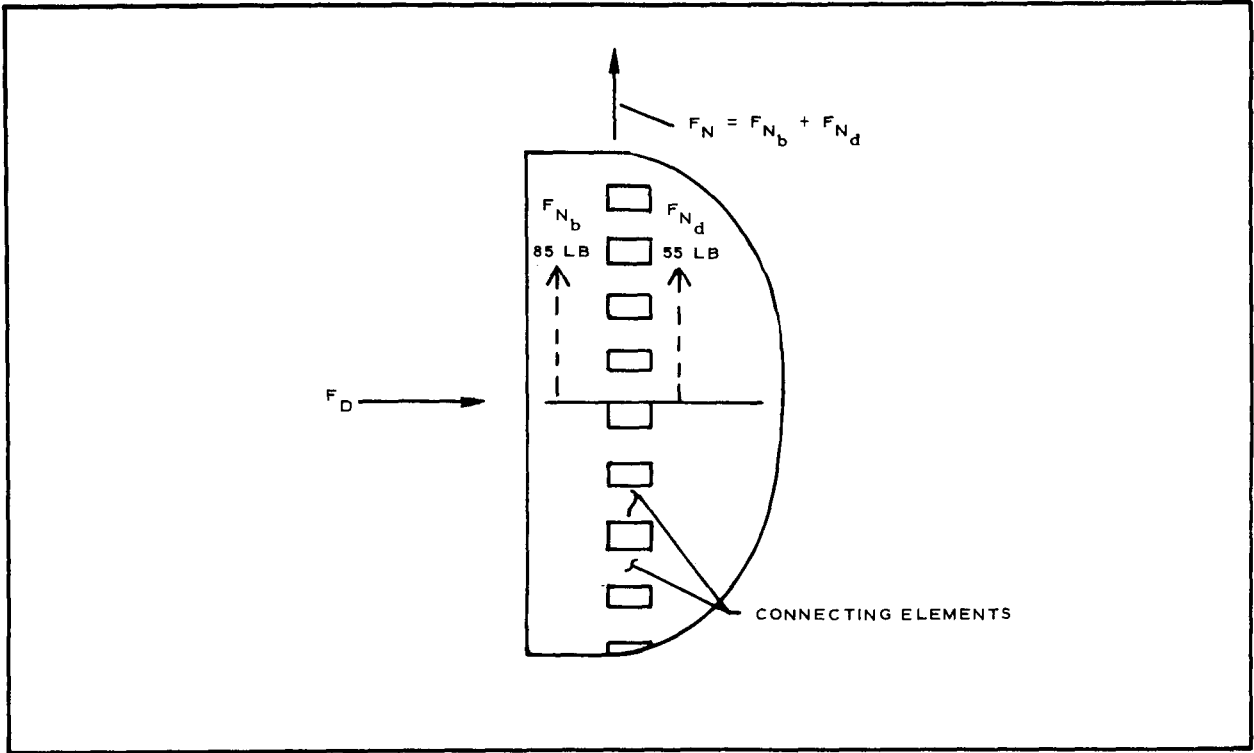


Figure 39 - Assumed Distribution of Normal Force

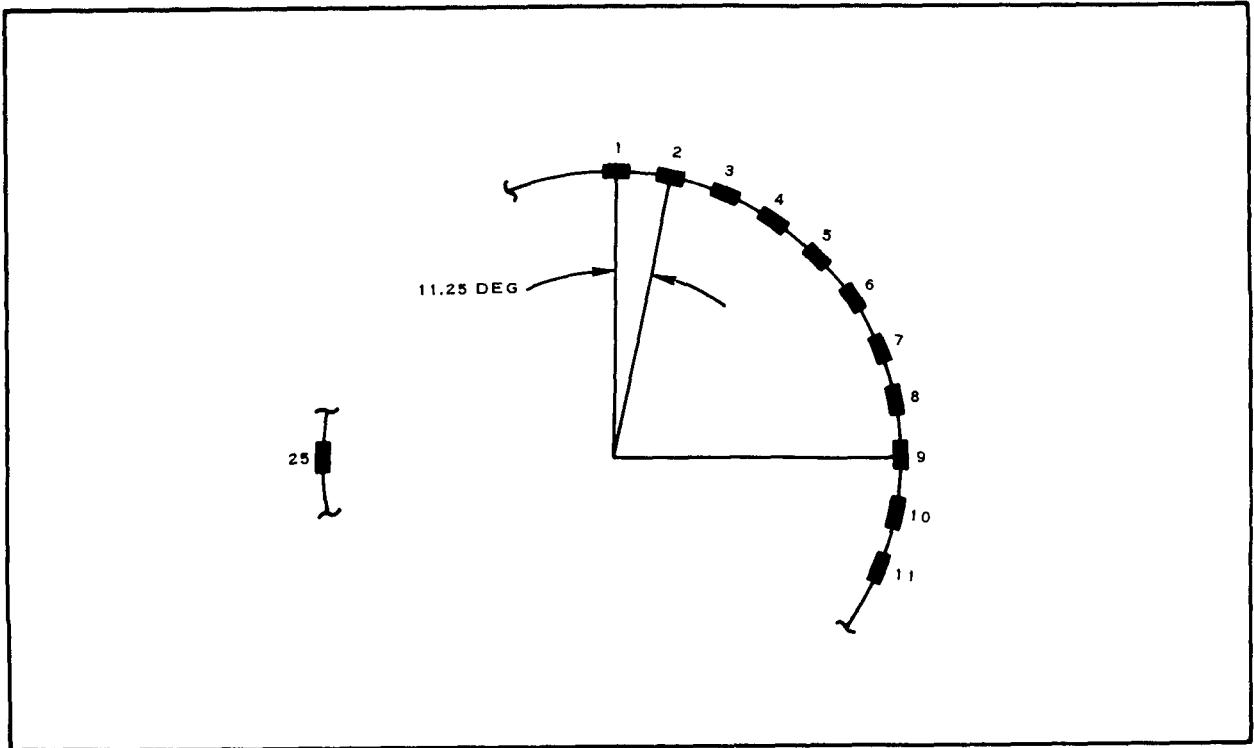


Figure 40 - Cross Section of Elements Connecting Disk and Band

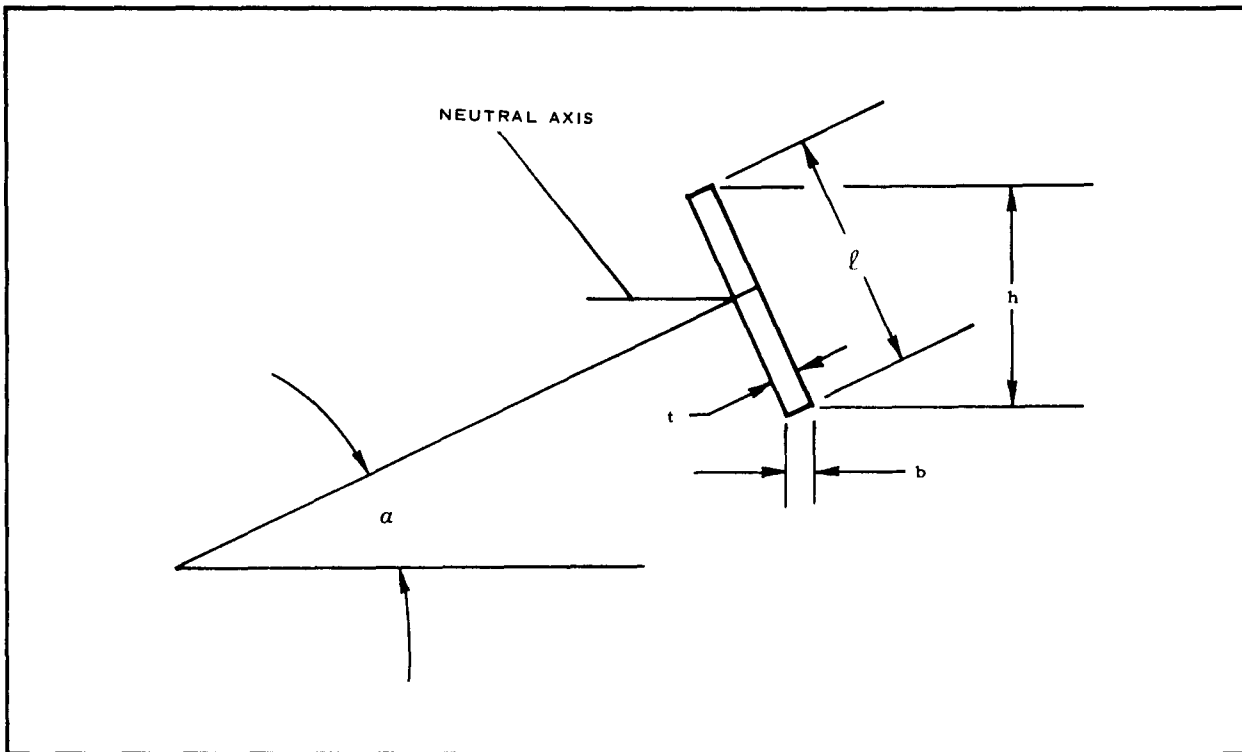


Figure 41 - Geometry of Connecting Element

$$\begin{aligned}
 I_{NA} &\approx \frac{lt^3}{12} \\
 &= \frac{(0.1)(0.063)^3}{12} \\
 &= 2.08 \times 10^{-6} \text{ in.}^4 .
 \end{aligned}$$

The moments of inertia for elements 1 through 9 are summarized in Table VIII.

The sum of the moments of inertia for the 32 elements is

$$\begin{aligned}
 I_s &= 2(I_1 + I_9) + 4(I_2 + \dots + I_8) \\
 &= 1.03 \times 10^{-4} \text{ in.}^4 .
 \end{aligned}$$

The approximate load carried by elements 9 and 25 can be determined from the relation

$$\begin{aligned}
 F_9 &= F_{25} \\
 &= \left(\frac{I_9}{I_s} \right) (F_{Nb}) ,
 \end{aligned}$$

$$= \frac{2.08 \times 10^{-6}}{1.03 \times 10^{-4}} \quad (85)$$

$$= 1.72 \text{ lb.}$$

The bending stress in Element 9 can now be determined from the relation,

$$f_b = \frac{Mc}{I} .$$

From the geometry of Element 9 (Figure 42) the maximum moment is

$$M = \frac{0.55}{z} \quad (1.72)$$

$$= 0.474 \text{ in. -lb .}$$

Therefore, the maximum bending stress in element 9 is

$$f_b \text{ max} = \frac{(0.474)(0.05)}{5.25 \times 10^{-6}}$$

$$= 4520 \text{ psi.}$$

The factor of safety, considering a 75,000 psi allowable, is

$$\text{F.S.} = \frac{75,000}{4,520}$$

$$= 16.6 .$$

TABLE VIII - MOMENTS OF INERTIA

Element	Moments of inertia (in. ⁴ × 10 ⁶)
1	2.08
2	2.08
3	2.08
4	2.08
5	2.62
6	3.63
7	4.48
8	5.05
9	5.25

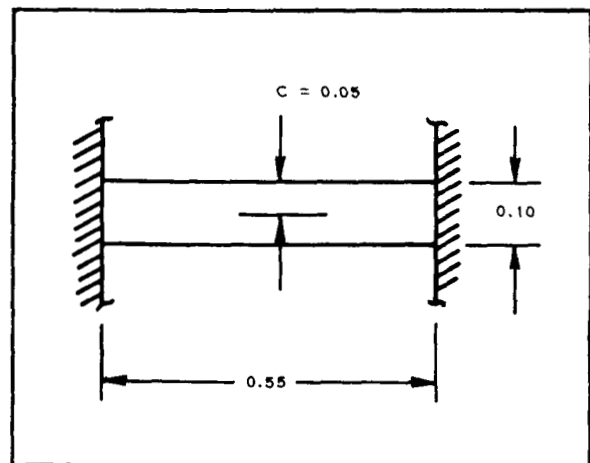


Figure 42 - Element 9

IV - DESIGN DOCUMENTATION

The design drawings for the decelerator models (fabric and pressure), deployment bags, riser, and bridle are presented in Figures 43 through 48. The drawing, assembly, and/or part numbers of each item are identified in Table IX.

TABLE IX - MAJOR DECELERATOR COMPONENTS

Figure number	Drawing number	Item	Assembly	Part number	Reefing
43	655A-001	10 percent DGB	-101	. . .	No
			-107	. . .	Yes
		12.5 percent DGB	-103	. . .	No
			-109	. . .	Yes
		15 percent DGB	-105	. . .	No
			-111	. . .	Yes
		Connector link	. . .	MS22002-1	. . .
Riser	. . .	-41	. . .		
		Swivel	. . .	GL1844A-1	. . .
		Bridle	-121
44	655A-002	Modified ringsail	-101
45	655A-003	Standard BALLUTE configuration	-111
		Modified BALLUTE configuration	-101
46	655A-005	Parachute deployment bag	-101
	655A-006	BALLUTE deployment bag	-101
47	655A-007	BALLUTE pressure model	-101
		DGB pressure model
		Internal measurements	-103
		External measurements	-105

This envelope contains:

Figure 43 - Disk-Gap-Band Parachute Assembly, 5.5-Ft D_o
(Drawing 655A-001, Sheet 1 of 4)

This envelope contains:

Figure 43 - Disk-Gap-Band Parachute Assembly, 5.5-Ft D_o
(Drawing 655A-001, Sheet 2 of 4)

This envelope contains:

Figure 43 - Disk-Gap-Band Parachute Assembly, 5.5-Ft D_o
(Drawing 655A-001, Sheet 3 of 4)

This envelope contains:

Figure 43 - Disk-Gap-Band Parachute Assembly, 5.5-Ft D_o
(Drawing 655A-001, Sheet 4 of 4)

This envelope contains:

Figure 44 - Ringsail Parachute Assembly, 5.5-Ft D_o
(Drawing 655A-002, Sheet 1 of 2)

This envelope contains:

Figure 44 - Ringsail Parachute Assembly, 5.5-Ft D_o
(Drawing 655A-002, Sheet 2 of 2)

This envelope contains:

Figure 45 - BALLUTE, 48-In. -Diameter Burble Fence
(Drawing 655A-003, Sheet 1 of 5)

This envelope contains:

Figure 45 - BALLUTE, 48-In. -Diameter Burble Fence
(Drawing 655A-003, Sheet 2 of 5)

This envelope contains:

Figure 45 - BALLUTE, 48-In. -Diameter Burble Fence
(Drawing 655A-003, Sheet 3 of 5)

This envelope contains:

Figure 45 - BALLUTE, 48-In. -Diameter Burble Fence
(Drawing 655A-003, Sheet 4 of 5)

This envelope contains:

Figure 45 - BALLUTE, 48-In. -Diameter Burble Fence
(Drawing 655A-003, Sheet 5 of 5)

This envelope contains:

Figure 46 - Parachute Deployment Bag (Drawing 655A-005)

This envelope contains:

Figure 47 - BALLUTE Deployment Bag (Drawing 655A-006)

This envelope contains:

Figure 48 - Disk-Gap-Band Parachute and BALLUTE Pressure Models
(Drawing 655A-007, Sheet 1 of 4)

This envelope contains:

Figure 48 - Disk-Gap-Band Parachute and BALLUTE Pressure Models
(Drawing 655A-007, Sheet 2 of 4)

This envelope contains:

Figure 48 - Disk-Gap-Band Parachute and BALLUTE Pressure Models
(Drawing 655A-007, Sheet 3 of 4)

This envelope contains:

Figure 48 - Disk-Gap-Band Parachute and BALLUTE Pressure Models
(Drawing 655A-007, Sheet 4 of 4)

V - MANUFACTURING CONSIDERATIONS

Because the performance of small-scale decelerators can be significantly affected by small variations in the fabrication process, particular emphasis was placed on maintaining high standards of workmanship during the program. In addition to the quality procedures typically instituted, the following additional precautions were taken to ensure maximum similarity between models of the same design.

1. Minimum realistic tolerances were maintained during each phase of the manufacturing process.
2. Manufacturing procedures were established that minimized unfavorable tolerance built up (tolerances were assigned on a plus-only basis where possible).
3. Fabric technicians with past experience in the manufacture of similar type decelerator models were used exclusively.
4. Each fabric technician was used in the same manufacturing capacity on each model.
5. Materials were maintained in a temperature- and humidity-controlled environment during fabrication to maintain a maximum degree of dimensional stability.
6. Detailed in-process inspections of each part fabricated were conducted to ensure that high standards of workmanship were maintained before assembly of the decelerator was initiated.

VI - CONCLUDING REMARKS

Continuing research and development activities, such as the current program, promise needed improvements in decelerator system capabilities. While the current program has focused on arriving at a better understanding of the performance aspects of the decelerator, it is believed a similar wind-tunnel effort investigating various structural efficiencies (e.g., design factors) for a single parachute configuration would be meaningful. The need for a technique to more precisely describe the loads sustained and stresses developed during the parachute deployment process is well recognized. Methods of analysis for the AID and BALLUTE (References 3 and 16), which take a well-defined shape due to their inflatable nonporous envelope, are at this time relatively well defined. The ultimate goal of developing such a technique for the parachute is, of course, its application to the design of flight systems and a reduction of future requirements for large-scale flight testing.

Results from the DGB tests of the current program offer a meaningful starting point in terms of filling times, inflated shapes, pressure distributions

(to be obtained from the DGB pressure model design), load-time histories, and basic design and fabrication techniques relating to this size decelerator.

APPENDIX A - BALLUTE INFLATION ANALYSIS

Inflation Model

Goodyear Aerospace has developed a theoretical method for estimating the fill time and inflation pressure of attached and towed BALLUTE decelerators. For towed configurations, an analytical model is used in which the inflating BALLUTE is considered to be a cone-sphere body. During inflation, the cone semi-apex angle varies between initially zero and the full-inflation value of 40 deg. The enclosed volume is assumed to vary as the cube of the sine of the semi-apex angle.

The method of analysis begins by determining aerodynamic characteristics along the surface of the BALLUTE configuration. A characteristic line is established which passes through the geometric center of the inflation inlet plane and intersects the BALLUTE envelope (see Figure 49). This line is defined such that the aerodynamic characteristics along the line are constant (neglecting momentarily the pressure of the inlet structure). The intersection of the characteristic line and the BALLUTE envelope is defined by the "inlet angle"

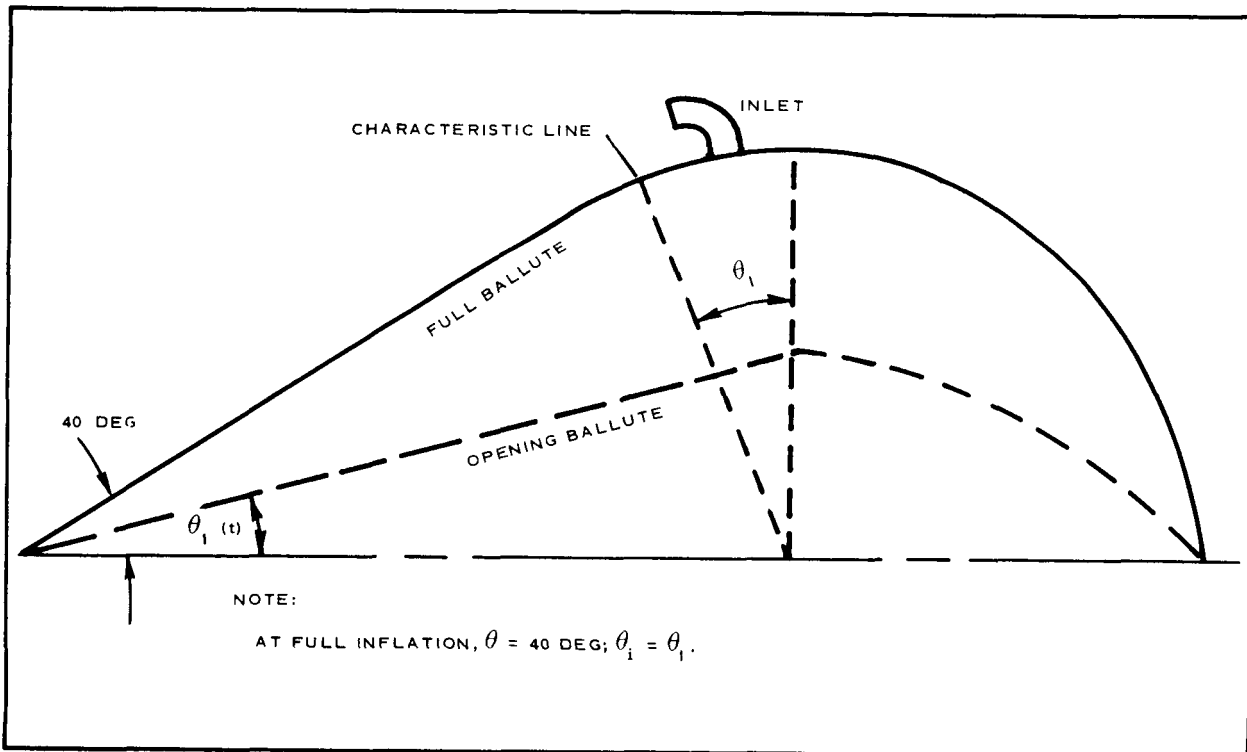


Figure 49 - BALLUTE Inflation Model

θ_i as shown in Figure 49. Throughout the filling process, the inlet axis (normal to the inlet plane) is assumed parallel to the BALLUTE surface and, hence, aligned with the flow. As a result, the inlet angle, θ_i , increases from zero at the start of inflation to a maximum constant value of θ_i at full inflation.

The model described above now can be used to determine the inflation time. Basically, the flow conditions into the inlet are obtained and an incremental mass flow into the BALLUTE is calculated over a small but finite time span. The resulting incremental mass is then added to the previous total value. With each iteration, a new BALLUTE volume is determined which is then used to define the new semi-vertex angle, θ . The fill time is also updated to correspond to the new volume and semi-vertex angle value. Iterations of this type are continued until the inflated volume corresponds to the fully-inflated BALLUTE volume and the calculated semi-vertex angle equals 40 deg. The corresponding time then defines the inflation time.

Calculating Procedure

In supersonic flow over the conical forward section, the shock wave is attached for a given Mach number up to a vertical semi-vertex angle θ_{crit} . If the semi-vertex angle is increased above this critical value or alternately if the Mach number is lowered, the shock wave will detach. As a result of this phenomenon, it can be shown that there are five flow cases which must be considered:

1. $\theta < \theta_i < \theta_{crit} < 40 \text{ deg}$
2. $\theta_i < \theta < \theta_{crit} < 40 \text{ deg}$
3. $\theta_i < \theta_{crit} < \theta < 40 \text{ deg}$
4. $\theta_{crit} < \theta < \theta_i < 40 \text{ deg}$
5. $\theta_{crit} < \theta_i < \theta < 40 \text{ deg}$

It should be pointed out that when $\theta = 40 \text{ deg}$, inflation is considered complete with respect to any further geometric changes of the BALLUTE shape. The internal pressure, however, may continue to increase.

For the first case, the shock wave is attached and the surface flow properties are obtained using a conical flow solution. If the flow forward of the inlet is supersonic, then a shock will result and subsonic conditions will exist as the flow enters the inlet. These inlet conditions can be obtained using normal shock relationships.

In the second case, the same computation procedure is employed except that the static pressure forward of the inlet is based on a conical flow solution using the inlet angle, θ_i , rather than the semi-vertex angle, θ .

For the third case, the shock at the nose is detached and the total pressure is determined from normal shock relationships. The static pressure in front of the inlet, however, is calculated using a conical flow solution as in the second case.

For the last two cases, the tangent-cone method employed in earlier cases is no longer meaningful. For these cases, then, a Newtonian approximation is used in which the pressure varies as a function of the equivalent semi-apex angle. The total pressure is found from normal shock relationships as in Case 3.

It should be noted that an inlet efficiency factor based on experimental data over a wide range Mach number and flow conditions is used. This factor compensates for random fluctuation in the inlet alignment as well as other factors unaccounted for in the idealized inflation model.

SYMBOLS

A	area
b	base, in.
c	chord length, in. ; line convergence factor
C_D	drag coefficient
e	abrasion factor
F_{Nb}	normal force on band, lb
F_{Nd}	normal force on disk, lb
f	stress, asymmetrical loading factor
H	shear force, lb
h	height, in.
I	moment of inertia, in. ⁴
j	safety factor
$\frac{jcb}{me}$	design factor
l	length, in.
M	moment, in. -lb
m	joint efficiency factor
M. S.	margin of safety
N	normal

P	load, lb, pressure
q	dynamic pressure, psf
R_{PD}	inflated disk radius, in.
r	radius, in.
S	area
T	tension force, lb
t	thickness, in.
v	vent
W	width, in.
Z	number of suspension lines
λ_g	geometric porosity, percent of S_o

Subscripts:

all	allowable
c	compression, crown
D	drag, disk
dev	developed
e	external
g	gap
H	horizontal component
i	inlet
l	lobe
N	normal
NA	neutral axis
o	nominal
r	radial direction

Sb	skirt band
s	slot, summation
ss	sail scoop
sl	suspension line
T	total
v	vent
vb	vent band
α	angle, deg
δ	bending stress, psi
θ	angle, deg
γ	angle, deg
∞	free-stream conditions

REFERENCES

1. Whitlock, C.H.; and Bendura, R.J.: Inflation and Performance of Three Parachute Configurations from Supersonic Flight Tests in a Low-Density Environment.
2. Gillis, C.L.: Aerodynamic Deceleration Systems for Space Missions. AIAA Fifth Annual Meeting, Philadelphia, Penna. October 1968, Paper No. AIAA 68-1081.
3. Mikulas, M.M., Jr.; and Bohon, H.L.: Summary of the Development Status of Attached Inflatable Decelerators. AIAA Second Aerodynamic Decelerator Systems Conference, El Centro, Calif., September 1968, Paper No. 68-929.
4. Barton, R.: Development of Attached Inflatable Decelerators for Supersonic Application. NASA CR-66613. Goodyear Aerospace, May 1968.
5. Galigher, Lawrence L.: Aerodynamic Characteristics of Ballutes and Disk-Gap-Band Parachutes at Mach Numbers from 1.8 to 3.7. AEDC-TR-69-245, November 1969.
6. Usry, J.W.: Performance of a Towed, 48-Inch-Diameter (121.92-Cm) Ballute Decelerator Tested in Free Flight at Mach Numbers from 4.2 to 0.4. NASA TN D-4943.

7. Lemki, Reinhold: Final Report, 40 Ft DGB Parachute. NASA CR-66587, G.T. Schjeldahl Company, October 13, 1967.
8. Chernowity, G., ed.: Performance and Design Criteria for Deployable Aerodynamic Decelerators. AF Flight Dynamics Laboratory, Wright Patterson AFB. ASD-TR-61-579, December 1963.
9. Stone, F.J.: Final Technical Report, 55-Ft-D_o Ringsail Parachute, Planetary Entry Parachute Program. NASA CR-66588, Pioneer Parachute Company, Inc., December 1967.
10. Wind Tunnel Test of Ballute Decelerators (Unpublished). Tullahoma, Tenn., Arnold Engineering Development Center, 1961.
11. Faurote, G.L.: Aerodynamic Stability and Heating Analysis of Payload/Ballute Combinations. GER-14154, Akron, Ohio, Goodyear Aerospace Corporation, December 1968.
12. Ballute, 48-In.-Diameter Drogue. Akron, Ohio, Goodyear Aerospace Drawing 573A001-008, October 1965.
13. Henke, D.W.: Establishment of an Unsymmetrical Wake Test Capability for Aerodynamic Decelerators. Vol II, Analysis of High Speed Axisymmetric Wakes and Parasonic Parachute Performance. Technical Report AFFDL-TR-67-192, Goodyear Aerospace Corporation, March 1968.
14. Lau, R.A.: Wake Analysis for Supersonic Decelerator Applications. Vol I, Theoretical Analysis and Correlation of Wind-Tunnel and Shallow-Water Tow Channel Results. GER-14330, Akron, Ohio, Goodyear Aerospace Corporation, October 1969.
15. Bloetscher, F.: Aerodynamic Deployable Decelerator Performance - Evaluation Program Phase II. Technical Report AFFDL-TR-67-25, Akron, Ohio, Goodyear Aerospace Corporation, April 1967.
16. Houtz, N.: Optimization of Inflatable Drag Devices by Isotenoid Design. AIAA Paper No. 64-437, First Annual AIAA Meeting, Washington, D.C., 29 June through 2 July 1964.
17. Pake, F.A.: A Method for Estimating the Fill Time and Inflation Pressure of an Aeroshell Ballute and a Trailing Ballute. GER-14151, Akron, Ohio, Goodyear Aerospace Corporation, December 1968.
18. Hoerner, S.F.: Fluid-Dynamic Drag. 1965.
19. Roark, R.J.: Formulas for Stress and Strain. Fourth Edition, 1965.
20. Thormaehlen, K.F.: Design and Strength Requirements for Wind Tunnel Models. AEDC Document QCP-000-21, March 1967.